

Time dependent temperature effects on methane production in Arctic peat soils

Jeanette Slettnes Grunnvåg

BIO-3950 Master thesis in Biology - May 2019



Time dependent temperature effects on methane production in Arctic peat soils

Jeanette Slettnes Grunnvåg. Faculty of Biosciences, Fisheries and Economics
Department of Arctic and Marine Biology.

15th of May 2019.

Supervisor: Alexander Tøsdal Tveit

Table of contents

List of Tables	i
List of Figures	ii
Acknowledgements	v
Abbreviations	vi
Abstract.....	1
1 Introduction	2
1.1 Arctic peatlands.....	2
1.2 Carbon cycling in Arctic peatlands	3
1.2.1 Polymer degradation.....	5
1.2.2 Fermentation	6
1.2.3 Methanogenesis.....	8
1.2.4 Methane oxidation and release to the atmosphere	10
1.2.5 Microbial loop and Necromass degradation	10
1.3 Effect of temperature on biological systems.....	10
1.3.1 Effect of temperature on enzymes.....	11
1.3.2 Effect of temperature on cells	13
1.3.3 Temperature effects on microbial communities.....	14
1.3.4 Community driven processes	15
1.4 Objective.....	15
1.5 Hypotheses	15
2 Materials and methods	17
2.1 Sampling and setup	17
2.2 Gas sampling and measurement.....	19
2.3 Determination of microbial growth.....	20
2.4 Extracellular enzyme assays	21
2.5 Determination of microbial community compositions.....	22
2.5.1 Sample preparation.....	22
2.5.2 Total nucleic acid extraction.....	22
2.5.3 DNA quantification and quality check	23
2.5.4 16S amplicon sequencing	23
2.5.5 Data analysis	24

3	Results.....	28
3.1	Chemical.....	28
3.1.1	Temperature log	28
3.1.2	Soil water content and pH.....	29
3.1.3	CH ₄ and CO ₂ production.....	29
3.1.4	Mass specific growth.....	33
3.1.5	Enzyme activity.....	34
3.2	Biological.....	36
3.2.1	DNA amounts as indicator of biomass.....	36
3.2.2	Community composition	37
3.2.3	Correspondence analysis	40
3.2.4	Abundances of influential OTUS from CA	43
4	Discussion	46
4.1	Incubation temperatures.....	46
4.2	Primers.....	46
4.3	Gas production	47
4.4	Growth rates.....	49
4.5	Community composition	50
4.6	Temperature range.....	52
5	Conclusion.....	53
6	Outlook.....	53
	References.....	54
	Appendix I: Materials and methods	63
	A Determination of microbial growth: DNA extraction protocol	63
	B Determination of microbial growth: DNA quantification with PicoGreen (Quanti-iT™ PicoGreen, Life Technologies).....	66
	C DNA quantification and quality check: Gels.....	68
	D 16S Amplicon sequencing: Percentage coverage of primers	69
	Appendix II: Results	70
	A Linear regression plot of CH ₄ concentrations	70
	B Biphasic CH ₄ production rates.....	71

List of Tables

Table 1 16S rRNA gene primer set used in PCR of samples.....	24
---	----

List of Figures

Figure 1 Global peatland distribution estimates of PEATMAP © (Xu, et al., 2018).....	2
Figure 2 Overview of degradation processes in peat. Each yellow box corresponds to metabolic processes, dark brown circle corresponds to the product of the metabolic processes and the white circles are the main monomers produced by the upstream decomposition. Modified from figure 4 of (Tveit, et al., 2013).	4
Figure 3 Schematic overview of hydrogenotrophic (black arrows), acetotrophic (blue arrows) and methylotrophic (green) methanogenesis. In hydrogenotrophic methanogenesis CO ₂ is reduced to CH ₄ through a series of steps which require coenzymes such as MFR, H ₄ MPT, F ₄₂₀ , CoM and CoB (Thauer, 2012). Acetotrophic methanogenesis involves the conversion of acetate to Acetyl-CoA which then enters the same pathway of hydrogenotrophic methanogenesis as methyl-H ₄ MPT. Methanol, methylamines and other C1-molecules of methylotrophic methanogenesis can either be converted to CH ₄ (~75%) or to CO ₂ (~25%) through reverse hydrogenotrophic methanogenesis.	9
Figure 4 The average air temperature over a year at Svalbard and 2-standard deviation error bars indicating the variation within each month. Based on temperature data from Adventdalen over the last 120 years. © Metrological institute of Norway.....	18
Figure 5 Schematic overview of the experimental setup of the temperature incubations.	19
Figure 6 Results of the temperature logging showing the real temperature and fluctuations for the incubations. Orange line shows the fluctuation in temperature of the 2°C incubations, cyan line shows fluctuation of 4°C incubation, purple line shows fluctuation at 6°C, dark red shows fluctuation at 8°C and dark blue shows fluctuation at 10°C.	28
Figure 7 Variation of water content (%) and pH in samples 1 to 17 at the end of incubation, sorted after which temperature treatment they received.....	29
Figure 8 Concentration of CH ₄ (μmol per ml soil slurry) as a function of time (days) with 95% confidence intervals. Data points are shown for all samples with a loess regression fitted and 95% confidence interval bands. Marked as grey are samples that remained at 2°C throughout the incubation, blue are samples that were changed from 2°C to 3°C at 15 days after incubation start and lastly to 5°C on day 22. The samples that were moved through all temperature incubations, from 2°C to 3°C after 15 days, to 5°C after 22 days, 7.5°C after 30 days and finally to 9°C, are marked in orange.	30
Figure 9 Arrhenius plot of (A) rates divided into beginning and acclimatized points (except for 2°C and 3°C) against 1/k _B T with a linear regression with slope 1.05 and a 95% CI shown in grey of [0.43-1.67], (B) ‘beginning’ points have been removed which resulted in a slope of 1.14, and a tighter 95% CI of [0.90-1.38] and (C) only beginning points with a linear regression (blue line) with slope 0.53 and a 95% of [-0.26 – 1.32] and a 3 rd degree polynomial (red line) to show a better fitted regression model. The 3°C was included in all three plots... ..	31
Figure 10 Concentration of CO ₂ (μmol per g dry soil) as a function of time (days) with 95% CI bands. Data points are shown for all samples with a loess regression fitted and 95% confidence interval bands. Marked as grey are samples that remained at 2°C throughout the incubation, blue are samples that were changed from 2°C to 3°C at 15 days after incubation	

start and lastly to 5°C on day 22. The samples that were moved through all temperature incubations, from 2°C to 3°C after 15 days, to 5°C after 22 days, 7.5°C after 30 days and finally to 9°C, are marked in orange.	32
Figure 11 Mass specific growth with 95% CI bars for the 2°C, 5 °C and 9 °C treatments. A Levene's test showed no homogeneity of the sample variances ($p = 0.57$).....	33
Figure 12 Arrhenius plot of (A) growth rates with outliers and a linear regression fitted with a 95% CI marked in grey, and (B) growth rates without outliers showing a linear regression (blue line) and a better fitting 2 nd degree polynomial.....	34
Figure 13 Potential enzyme activities of (a) beta-glucosidase and (b) leucine-aminopeptidase for 2-, 5- and 9°C samples. Note: activity measurements were performed on 4 samples for each temperature. The measurement was performed at 6°C for all 12 samples.	35
Figure 14 The amounts of DNA from extractions in ng of DNA per g of soil separated into start and end samples. Samples at 2°C marked in grey, samples of the 5°C treatment marked in blue, and samples of the 9°C treatment marked in orange.	36
Figure 15 Distribution of abundances of the phyla representing >10% of the total data set. Faceted into start and end samples to visualise the relationship between time, temperature and the bacterial community composition.....	38
Figure 16 Distribution of abundances of all the phyla within the Archaea. Faceted into start and end samples to visualise the relationship between time, temperature and the archaeal community composition.	39
Figure 17 Abundance distribution of the classes represented within the Euryarchaeota phylum between start and finish and sorted for the temperature treatments, to visualise t the relationship between time, temperature and the archaeal community composition.	40
Figure 18 Correspondence analysis of (A) bacterial OTUs (99% threshold) and (B) archaeal OTUs (95% threshold). Start samples are marked as circle, end samples as open triangles. Green are the samples undergoing the 9°C treatment, red are the 5°C control samples and black are 2°C control samples. Sample E4 (2°C control sample) was removed from the CA.	42
Figure 19 Abundance plot of the most influential OTUs of the Bacteria (A) pulling the start samples in the negative direction of the x-axis, and (B) pulling the end samples in the positive direction of the x-axis of the CA plot.	43
Figure 20 Abundance plot of the most influential OTUs of the Archaea (A) pulling the start samples towards the positive direction of the y-axis, and (B) pulling the end samples in the negative direction of the y-axis of the CA plots.	45
Figure 21 Proposed balance between carbon being used for biomass growth, CH ₄ production and necromass degradation. Before temperature change (black arrows) carbon is sequestered into both biomass growth and CH ₄ production. After the temperature increase more carbon is going into both the biomass and the CH ₄ production (red, solid lines), but the number of deaths caused by predation and viral infection has not caught up, leading to the same amount of carbon going from the necromass into CH ₄ production as before temperature change (red, dotted lines). When predators and viral infections catch up the death rates increase and as a response, necromass degraders starts feeding more carbon into the production of CH ₄ (blue lines).	52

Figure 22 Quality check of the DNA of the extraction replicates of the start samples. Replicate 1 of S1 had a smear and was subsequently not used for the 16S amplicon sequencing. All other replicates showed DNA bands.	68
Figure 23 Quality check of the DNA of the extraction replicates of the end samples. All replicates showed DNA bands.	68
Figure 24 Linear regression models fitted for each temperature treatment. Red is for the 2°C incubations, yellow is for the 3°C incubations, green is the 5°C incubations, blue is the 7.5°C incubations and purple is for the 9°C incubations.	70
Figure 25 The average concentration of CH ₄ for each temperature treatments plotted against time. Black, stippled lines shows how the biphasic rates were calculated. These are not exact, just indications of how it was done. All samples of the 2°C were plotted along with the average to confirm that the average was a good representation of all the samples. The rates for the 2°C and 3°C were not treated as biphasic.	71

Acknowledgements

First and foremost, I would like to thank my supervisor Alexander Tveit for his advice and guidance throughout my thesis. Your good mood and positivity have made the process so much more enjoyable.

A very special thank you to Kathrin, you have been a great support both in helping me in the lab, with analysing the data and just as someone to talk to in general. It has been so valuable having the support of someone who has recently been through the same process of writing and conducting a master thesis.

Thank you to Alena and Anne Grete for your help in the lab, Dimitri for the bioinformatics script and help with it, MaiaLEN for suggesting the Arrhenius calculations and everyone else in the Methane group and the extended Microplant group.

Thank you to the people at the department of Terrestrial Ecosystem Research at the University of Vienna for making my stay during the spring of 2018 so pleasant. Special thanks to Margarete Watzka, Yuntao Hu and Ludwig Seidl for processing my samples and notably Vicky Martin for all her knowledge and for helping with the ^{18}O and the enzyme assay when my time in Vienna was not enough to do everything.

Thank you to Aslak and Alicia for being my best office buddies!

Lastly, thank you to my family for being profoundly confused but at the same time interested when I talk about my studies.

And Gabriel, you are invaluable to me.

Abbreviations

AMC	aminomethylcoumarin
ATP	adenosine triphosphate
CH₄	methane gas
CHO	formyl group
CI	chloroform isoamylalcohol
CoA	coenzyme A
CoB	coenzyme B
CoM	coenzyme M
CO₂	carbon dioxide gas
CTAB	cetyltrimethylammonium bromide
DEPC	diethyl pyrocarbonate
DNA	deoxyribonucleic acid
EtOH	ethanol
GHG	greenhouse gases
Gt	gigatonnes
H₂	hydrogen gas
H₄MPT	tetrahydromethanopterin
K₂HPO₄	dipotassium phosphate
Mcr	methyl-coenzyme M reductase
MFR	methanofuran
MUF	methylumbelliferyl
N₂	nitrogen gas
NADH	nicotinamide adenine phosphate
NADPH	nicotinamide adenine dinucleotide phosphate
-SH	sulphydryl
SOC	soil organic carbon
O₂	oxygen gas
PCI	phenol chloroform isoamylalchohol
PCR	polymerase chain reaction
PEG	polyethylene glycol
RNA	ribonucleid acid
rRNA	ribosomal RNA

Abstract

Peatlands constitute the largest natural reservoir of carbon on the planet making them key components in the global carbon balance. Peatlands are mostly found in the northern hemisphere under cold conditions. As the world is warming and arctic peatlands are becoming heavily influenced by increasing temperatures, an increased interest in the peat soil microbial systems have arisen. Methane, a potent climate gas, is produced in the anaerobic environment of peatlands by methanogenic archaea which are supplied with carbon, energy and nutrients through a complex network of microbes. How these communities are influenced by changes in temperature is crucial for our understanding on the effects of climate change. In this master thesis the effect of gradually increasing temperatures on CH₄ producing microorganisms in Arctic peat was studied within a seasonal timescale. The major aim was to provide a better understanding of how CH₄ producing microorganisms in peat react to temperature changes over time. Multiple incubations were set up and gradually moved from 2°C to 9°C, through 3, 5 and 7.5°C. Throughout the incubations gas measurements and samples for chemical analysis were collected. Analysis of growth and enzyme activity was performed at the end of the experiment. Analyses of 16S rRNA genes were performed for samples at the start and end of incubation. Only small changes in the community composition were observed and no differences in the biomass between the start and end, or between temperature treatments. There was also no difference in the extracellular enzyme activity for the different temperature treatments. The CO₂ production showed the same trend for all treatments throughout the experiment, while the CH₄ production demonstrated a clear temperature dependence. Furthermore, using the Arrhenius equation it was shown that the temperature dependence of CH₄ production rates as well as the growth rates for the whole community were comparable to that of pure culture of methanogens, but that the rates right after temperature change were not in accordance with the Arrhenius equation. This demonstrates that biological adaptations occur directly after temperature change. We suggest that this biological acclimatization is in part a result of initial biomass buildup after temperature change that is subsequently balanced by cell death and necromass degradation feeding into CH₄ production. Alterations in the microbial loop in the short-term might help to explain the microbial community changes observed and why the temperature effects on CH₄ production in these Arctic peat soils are time-dependent.

Keywords:

Temperature effects, methanogens, peatland, CH₄ production, temperature dependence, necromass, biomass, adaptation over time, Arrhenius.

1 Introduction

1.1 Arctic peatlands

Peatlands cover about 3% of Earth's land surface area and exists at all latitudes but are mostly found in the northern hemisphere (figure 1) (Xu, et al., 2018). Peatlands are estimated to contain 400 – 600 gigatonnes (Gt) of carbon (Tarnocai, et al., 2009; Yu, et al., 2010; Page, et al., 2011; Yu, 2012), amounting to about one third of the global soil organic carbon (SOC) (Joosten & Couwenberg, 2008; Strack, et al., 2008). This makes peatlands the largest natural reservoirs of carbon on the planet. Peatlands are important carbon dioxide (CO_2) sinks and sources of methane (CH_4) emissions to the atmosphere (Strack, et al., 2008) and thus important for the global carbon balance.

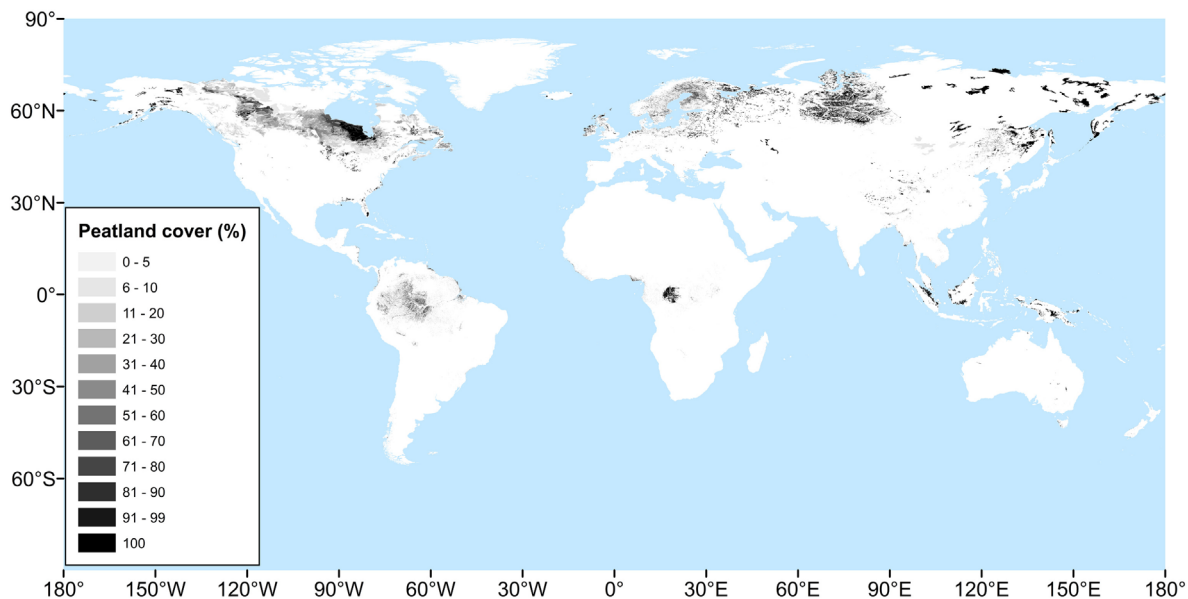


Figure 1 Global peatland distribution estimates of PEATMAP © (Xu, et al., 2018).

In the polar and circumpolar regions of the northern hemisphere much of the carbon is sealed in permafrost (Tarnocai, et al., 2009). Permafrost soils are defined as soils that have remained below 0°C for at least two consecutive years (Permafrost Subcommittee, 1988). The layer above the permafrost, which is termed the active layer, thaw during spring and re-freeze during autumn. The active layer has a higher microbial activity and biomass compared to the permafrost layer below (Hultman, et al., 2015). Many Arctic peatlands form when the underlying permafrost hinders water drainage, causing the subsurface active layer to become

waterlogged. This water saturation, along with a high content of intact and partially degraded organic material, are the main characteristics of peatlands (Xu, et al., 2018; Strack, et al., 2008). Due to the high water content, a combination of solubility limitations, mass transfer limitations and microbial respiration reduces oxygen (O_2) concentrations with depth, resulting in most of the soil column being anaerobic.

Dead organic plant material accumulates in peat soils because of an imbalance between the production of new organic material and decomposition of dead matter (Frolking, et al., 2011). The rate of this accumulation is dependent on the speed of plant growth relative to the microbial decomposition rate. The degradation processes are limited by the lack of oxygen as an electron acceptor, low temperature, low pH and limited nutrient availability (McLatchey & Reddy, 1998). It has been suggested that microbial decomposition activities are constrained primarily due to high concentrations of phenolic compounds which inhibits microbial enzymes (Freeman, et al., 2001; Fenner & Freeman, 2011). Phenolic compounds can be degraded by phenol oxidases, but these enzymes require O_2 and are therefore not functional under anaerobic conditions, (McLatchey & Reddy, 1998) causing the accumulation of phenolics in the waterlogged peatlands.

Arctic peatlands are exposed to long winters at sub-zero temperatures, and short and cold summers. However, in the era of man-made global warming, the Arctic is warming faster than other regions of the world (Anisimov, 2007), a phenomenon called polar amplification (Bekryaev, et al., 2010; Holland & Bitz, 2003). There is growing concern that the efflux of greenhouse gases (GHG) from peatlands will increase as a result of increased temperatures that lead to thawing of permafrost, drought and peat fires (Strack, et al., 2008). Elevated emissions of Arctic peat carbon in the form of microbially produced CH_4 and CO_2 could have a considerable impact on the greenhouse gas content in the atmosphere. It is therefore imperative that we understand how microbial ecosystems in Arctic peatlands react to climate change.

1.2 Carbon cycling in Arctic peatlands

Methane is considered to be the one of the most important GHG after CO_2 in global warming (Myhre, et al., 2013). Methane has a lifetime in the atmosphere of about 10-12 years (Myhre, et al., 2013), and hence a shorter life-time compared to CO_2 , which stays in the atmosphere for about 100 years (Solomon, et al., 2007). However, CH_4 is a more potent climate gas and has 28

times the global warming potential of CO₂ over a time frame of 100 years on a weight to weight basis, which takes into account both the ability of the gases to absorb and emit infrared radiation and its lifetime in the atmosphere (Myhre, et al., 2013).

CH₄ is produced geologically either by the breakdown of organic matter at elevated temperatures and pressure, called thermogenic CH₄ formation (Schoell, 1988), or abiotically involving inorganic compounds in magmatic processes or via gas-water-rock reactions (Etiope & Lollar, 2013). Biogenic sources for CH₄ include both natural and anthropogenic systems. Major anthropogenic sources are livestock farming (Thornton, 2010), rice paddies, coal mining, landfills, wastewaters and fossil fuel production (Blaha, et al., 1999; Bousquet, et al., 2006). The largest natural source of CH₄ is biogenic production by methanogenic archaea (methanogens) in anoxic environments such as wetlands and marshes (Bousquet, et al., 2006).

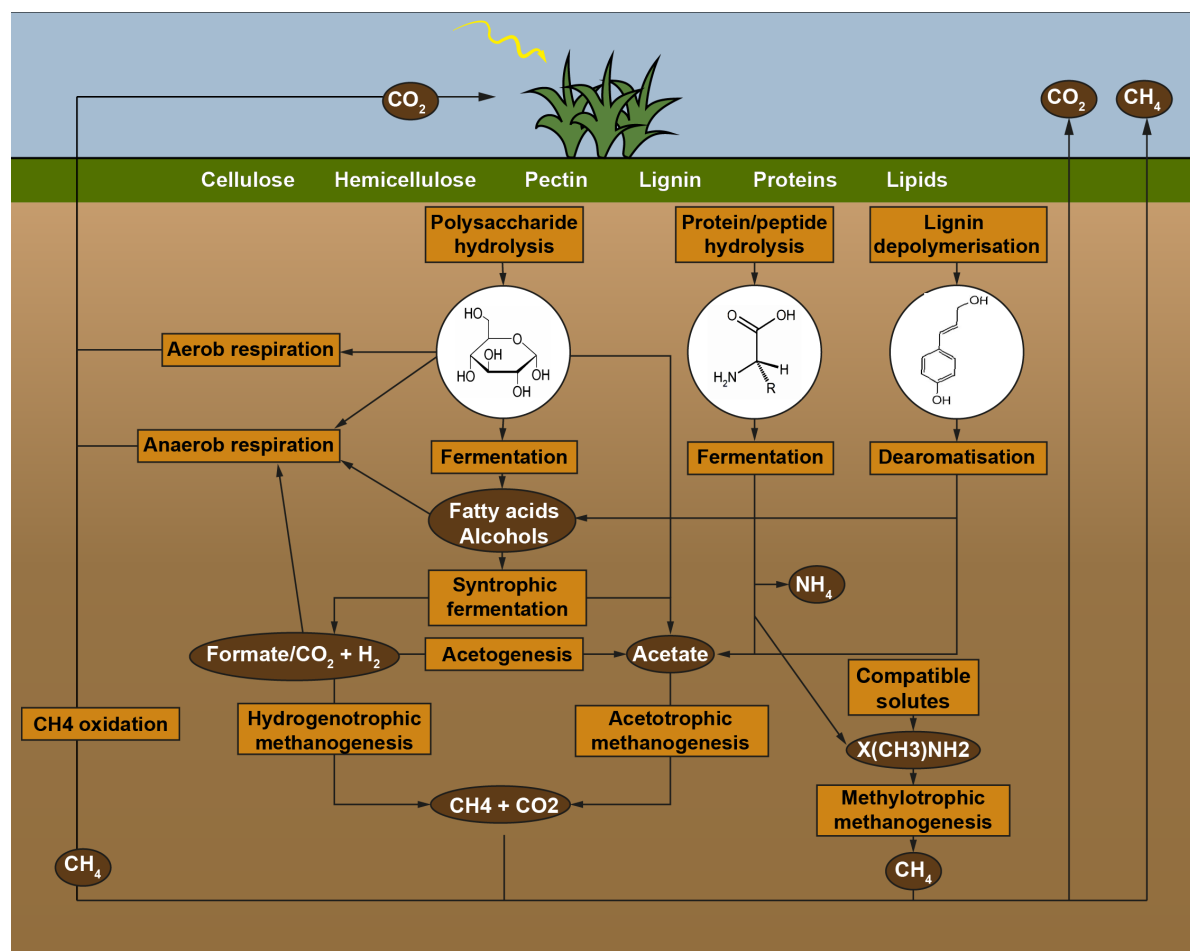


Figure 2 Overview of degradation processes in peat. Each yellow box corresponds to metabolic processes, dark brown circle corresponds to the product of the metabolic processes and the white circles are the main monomers produced by the upstream decomposition. Modified from figure 4 of (Tveit, et al., 2013).

Methanogens can use certain substrates as carbon and energy sources: acetate, CO₂ and H₂, and C1 compounds including methanol and mono-, di- and tri-methylamines (Whitman, et al., 2006). These substrates are supplied to the methanogens through a network of microbial decomposition where complex organic matter including polysaccharides, proteins and lignin is degraded into smaller molecules by a broad range of Bacteria with different metabolisms (figure 2).

1.2.1 Polymer degradation

In arctic peatlands grasses and mosses make up the majority of the plant cover (Noble, et al., 2019; Breeuwer, et al., 2009). Plants use solar energy to yield high-energy chemical compounds such as adenosine triphosphate (ATP) and nicotinamide adenine dinucleotide phosphate (NADPH) which are used in the Calvin cycle to fix CO₂ to synthesize sugars that are assimilated into complex polymers essential for the growth and maintenance of the plant (Freeman & Macmillan, 2013). Plant cells are composed of a cell wall, a large component of the plant cell, that surrounds membrane polymers and other cell constituents made up of carbohydrates, proteins and lipids. The cell wall consists of the polymer cellulose, along with pectin, hemicellulose, lignin as well as several proteins which all cross-link into a complex three-dimensional matrix (Keegstra, 2010). These polymers are unavailable for any bacterial decomposers as long as the plant is still alive, but as the plant dies, these compounds become available for microbial decomposition. The polymer degradation process is initiated by microorganisms that excrete polymer degrading enzymes (figure 2).

The major polymer cellulose is a polysaccharide that is hydrolysed into oligo- and monosaccharides (figure 2) by a type of enzymes called cellulases. There are several types of cellulases, e.g. Endocellulases that catalyse the hydrolysis of the β -(1→4) glycosidic bonds of cellulose, exocellulases which cleaves at the ends of the exposed cellulose chain to create tetra- or disaccharides (Lynd, et al., 2002), and β -glucosidases which hydrolyse the exocellulase products further into singular monosaccharides (Lynd, et al., 2002). Pectins and hemicelluloses are also polysaccharides, but are structurally heterogenous, composed of multiple different monosaccharides in addition to glucose (Sarkar, et al., 2009). Cleavage of the bonds in these compounds require several different enzymes (Sun, et al., 2012). There are many fungi and

Bacteria, and even some Archaea that express cellulases and utilize cellulose as a carbon and energy source (Lynd, et al., 2002). Tveit et al. (2015) reported a low abundance of fungi in anoxic peat from Svalbard compared to that observed in the upper oxic layers (Tveit, et al., 2013), which indicates a higher importance of bacterial groups in this process in the deeper layers of Arctic peat. The same report indicated members of the phyla Actinobacteria, Verrucomicrobia and Bacteroidetes as the main polymer degraders in the peat soil of Svalbard. When later considering only the anoxic peat soil, this was modified to Actinobacteria, Firmicutes and Bacteroidetes (Tveit et al. 2015).

Degradation of proteins (figure 2) occurs by hydrolysis of the peptide bonds between amino acids in peptide chains (Petsko & Ringe, 2009). A wide array of enzymes are responsible for proteolysis, e.g. aminopeptidases which cleaves off amino acids at the N-terminus of the protein (Gonzales & Robert-Baudouy, 1996; Taylor, 1993). Many proteases are ubiquitous and not very specific, but can have a higher affinity for some residues, for instance the leucine aminopeptidase which reacts fastest when cleaving off leucine residues (Gonzales & Robert-Baudouy, 1996). Soil Bacteria and fungi excrete proteases into the environment to decompose available proteins. The resulting amino acids can then be attained by the microorganisms and used as a carbon, nitrogen and energy source for growth or maintenance inside the cell.

Lignin is a polymer consisting of multiple units of phenolic compounds and is most abundantly distributed in secondary cell wall structures (Van Acker, et al., 2013) of for instance grasses. Mosses do not contain lignin (Sarkar, et al., 2009). Both fungi and Bacteria are known to break down lignin, but the process has been more deeply studied in fungi (Janusz, et al., 2017). Lignin-degrading Bacteria has been mainly found in the phylum Actinobacteria, and the α - and γ -Proteobacteria (Bugg, et al., 2011). Peroxidases and phenol oxidases (also called laccases) are two enzymes that are involved in lignin degradation (Bugg, et al., 2011), the latter of which requires O₂.

1.2.2 Fermentation

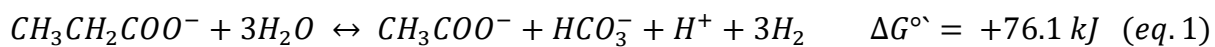
Fermentation is a form of energy metabolism without the use of an electron transport chain, as opposed to aerobic and anaerobic respiration. This type of metabolism is more common in environments where electron acceptors are depleted (Madigan, et al., 2015). Following polymer degradation, monosaccharides, amino acids and phenolics are acted upon by primary fermenters

to produce fatty acids such as acetate, propionate and butyrate, alcohols and hydrogen (H_2) - and CO_2 gas (Tveit, et al., 2015). Acetate and the gasses H_2 and CO_2 can be used directly by acetotrophic methanogens and hydrogenotrophic methanogens, respectively, to produce CH_4 and CO_2 (Tveit, et al., 2015).

Through sugar fermentation ATP is generated solely by the glycolysis pathway which converts glucose to pyruvate (Madigan, et al., 2015). Importantly, for the glycolysis to be maintained the oxidized version of the electron carrier NADH (NAD^+) needs to be regenerated. To do this pyruvate is reduced to produce molecules such as commonly known lactic acid or ethanol, but also many other types of alcohols, and fatty acids such as butyrate, propionate (Madigan, et al., 2015; Tveit, 2014) or oxidized to acetyl-CoA to from acetate (Tveit, 2014). In many of these types of fermentation the electrons are transferred to ferredoxin and further oxidized by hydrogenase to H_2 (Valentine & Wolfe, 1963).

Amino acid fermentation is not very well studied, and little is known about specific pathways and the functions in the environment. However, main products are generally ammonia, CO_2 and H_2 and acetate (Ramsay & Pullammanappallil, 2001) . It could also lead to the production of methylamines which are utilized by methylotrophic methanogens (Tveit, 2014). Aromatic compounds can be degraded through fermentative processes but are usually not thermodynamically favourable unless products are being depleted from the environment by syntrophic partners (Tveit, 2014).

After primary fermentation a large part of the polymeric carbon has been transformed into alcohols and fatty acids which cannot be used by most methanogens. These compounds are further metabolised by secondary fermenters to acetate or H_2 and CO_2 , which are substrates for the majority of methanogens. Most secondary fermenters depend on syntrophic partners such as methanogens for removal of hydrogen, formate and acetate produced during breakdown of the short chain fatty acids and alcohols (Conrad, 1999). The reason for this is that by lowering the product concentration, highly unfavourable reactions such as the conversion of propionate to acetate (eq.1) become thermodynamically favourable, e.g. in the syntrophic oxidation of propionate by a bacterium in syntropy with a H_2 utilizing methanogen (Mucha, et al., 1988).



1.2.3 Methanogenesis

To date, seven orders of methanogenic Archaea are known, where five of them are only known to contain hydrogenotrophic methanogens (Methanopyrales, Methanococcales, Methanobacteriales, Methanomicrobiales and Methanocellales). Members of the order Methanomasiliicoccales constitute, as far as we know, only obligate methylotrophic methanogens, while the Methanosarcinales is the most diverse group with members that perform both hydrogenotrophic, acetotrophic and methylotrophic methanogenesis (Buan, 2018).

All known methanogens are obligate anaerobes and produce CH₄ as a waste product of their metabolism. They can be found in anoxic environments such as wetlands and marshes, sediments and the intestinal tract of ruminants (Thauer, et al., 2008). Where there are high concentrations of sulphate, nitrate, manganese and iron, methanogens are usually outcompeted by Bacteria utilizing these substances (Thauer, et al., 2008) and are therefore mostly found in reduced environments. In Arctic peat from Svalbard the Methanosarcinales, Methanobacteriales and Methanomicrobiales are the most dominant orders of methanogens (Tveit, et al., 2013).

Hydrogenotrophic methanogens utilize CO₂ and most commonly H₂ as an electron source for reduction (Enzmann, et al., 2018). Some also use formic acid and sometimes alcohols for energy production (Zabranska & Pokorna, 2018; Thauer, 2012; Enzmann, et al., 2018). The reduction of CO₂ to CH₄ is a cyclical process where the first step, reduction of CO₂ to formyl-methanofuran (CHO-MFR) (figure 3.1), and the last step, reduction of Coenzyme B–Coenzyme M–heterodisulfide (CoM-S-S-CoB) to Sulphydryl CoB (HS-CoB) and Sulphydryl CoM (HS-CoM) (figure 3.7), is coupled.

Acetotrophic methanogenesis uses acetate for energy production and growth and is the largest contributor to CH₄ production in the biosphere (Ferry, 2010). The process happens through the transfer of a phosphate group and coenzyme A from ATP and Sulphydryl CoA (HS-CoA) to acetate to produce acetyl-CoA (blue pathway, figure 3). The methyl group of acetyl-CoA is then transferred to tetrahydromethanopterin (H₄MPT), and further converted to CH₄ as in hydrogenotrophic methanogenesis (figure 3) (Enzmann, et al., 2018). The remaining CO of the acetate is oxidized to CO₂.

A third way of CH₄ production is methylotrophic methanogenesis which utilizes C1-compounds that are methylated (green pathway figure 3). The methyl group of the compounds is transferred to Coenzyme M through a two-step methyltransferase pathway (Zydowsky, et al., 1987). Next, the methylotrophic methanogen either reduces the methyl-CoM to CH₄ (figure 3.7) or uses parts of the reverse methanogenesis pathway to oxidize the methyl-CoM to CO₂ (Timmers, et al., 2017).

The last step (figure 3.7) which produces CH₄ from methyl-coenzyme M is common for all methanogens and the gene coding for the α -subunit of the methyl-coenzyme M reductase (Mcr) which catalyzes the reaction is therefore commonly used as a phylogenetic marker for methanogens. All methanogenic pathways lead to the production of both a proton (H⁺) and sodium (Na⁺) ion gradient, which are used for ATP synthesis by the membrane-bound A₁A_O-ATP synthase (McMillan, et al., 2011; Mayer, et al., 2015).

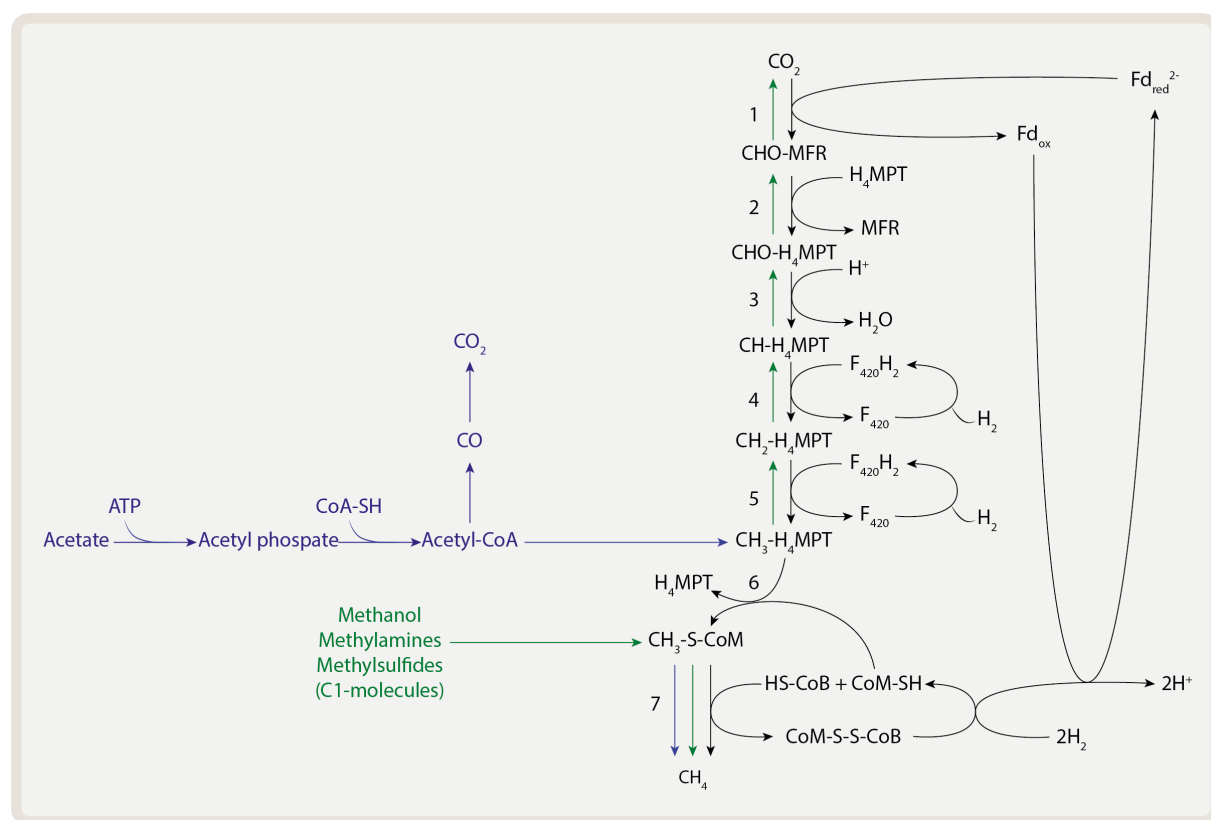


Figure 3 Schematic overview of hydrogenotrophic (black arrows), acetotrophic (blue arrows) and methylotrophic (green) methanogenesis. In hydrogenotrophic methanogenesis CO₂ is reduced to CH₄ through a series of steps which require coenzymes such as MFR, H₄MPT, F₄₂₀, CoM and CoB (Thauer, 2012). Acetotrophic methanogenesis involves the conversion of acetate to Acetyl-CoA which then enters the same pathway of hydrogenotrophic methanogenesis as methyl-H₄MPT. Methanol, methylamines and other C1-molecules of methylotrophic methanogenesis can either be converted to CH₄ (~75%) or to CO₂ (~25%) through reverse hydrogenotrophic methanogenesis.

1.2.4 Methane oxidation and release to the atmosphere

The gases produced by methanogenesis in deeper peat or other soil layers diffuses to upper and more oxic layers where the CH₄ is trapped and oxidized by methanotrophic Bacteria to form biomass and CO₂ or released into the atmosphere. Most CH₄ oxidizing Bacteria requires oxygen and is therefore found in the top oxic soil layers (Murrell, 2010). However, there is also evidence of anaerobic CH₄ oxidation by some Archaea (Pancost, et al., 2000; Schouten, et al., 2003; Schouten, et al., 2001) and Bacteria (Oswald, et al., 2017). A large fraction of the CH₄ produced by methanogens is oxidised by methanotrophic organisms (Reeburgh, 2007), but the residual CH₄ and the CO₂ produced is released to the atmosphere where they act as green-house gases.

1.2.5 Microbial loop and Necromass degradation

While the majority of energy and carbon transformed in anoxic peat ecosystems originates from the degradation of plant litter, a substantial proportion comes from microbial necromass (dead microbial cells). A large amount of these deaths arises from grazing and predation on the Bacteria and Archaea by eukaryotic, predatory protists and nematodes, as well as some predatory Bacteria for instance belonging to the Bacteroidetes (Lueders, et al., 2006). In addition, there are viruses that can infect and lyse bacterial and archaeal host organisms (Bratbak, et al., 1994). Death of the organisms makes the cell constituents of these dead cells become available for degradation by living cells, including cell wall polysaccharides, lipids, proteins and nucleic acids. Effectively, these molecules become integrated into the cell biomass or used for the production of energy which release compounds into the cycling of nutrients. Whether the living microbial biomass will increase will depend on the relationship between the rate of deaths to the rate of growth (Bradley, et al., 2018). There have been indications of Bacteroidetes among a limited number of phyla being responsible for mineralization of dead biomass in a fjord system in Svalbard (Müller, et al., 2018), and Planctomycetes responding with increased abundances in the presence of extracellular DNA (Morrissey, et al., 2015).

1.3 Effect of temperature on biological systems

Temperature is a physical measurement of hotness or coldness, and affects the phase, density and solubility properties of matter, the rate of chemical reactions and the amount of heat

radiating from or to an object. When the kinetic energy of atoms and molecules increase these will gain increased motion. The more motion the system has the higher the temperature of that system will be. This also increases the possibility of collisions between particles and the particles having enough energy to break their old bonds, making the rate of chemical reactions higher with increased temperatures.

1.3.1 Effect of temperature on enzymes

Like any chemical reactions, enzyme-catalyzed reaction rates increase as the temperature increases. If the temperature becomes too high the enzymes will denature and lose their activity. At temperatures below zero, enzymes might lose their activity completely if the water around them freezes. Typically, enzymes have a range of temperatures where they function optimally (Feller & Gerday, 2003). Different enzyme adaptations have made it possible for organisms to optimize their life to different temperatures. Examples of structural modifications that can bring more flexibility to an enzyme are reduction of cysteine residues that can form disulfide bridges, reduction in proline content and a higher amount of glycine and less hydrophobic and ionic interactions. As an example, a high lysine-to-arginine ratio has been seen to conformationally destabilize a cold adapted α -amylase (Siddiqui, et al., 2006). Generally, a reduction in residues that can form strong interactions with each other or the environment will have negative impact on the stability of an enzyme. As a consequence of higher flexibility, cold-adapted enzymes have efficient catalytic activity at low temperatures. For high temperatures the case is often opposite, where a more rigid structure will keep the enzyme from denaturing (Radestock & Gohlke, 2011).

1.3.1.1 The Arrhenius equation

The Arrhenius equation is a formula that describes the temperature dependency of a chemical reaction. Using the Boltzmann constant, the formula is given as:

$$r = A e^{\frac{-E_a}{k_B T}} \quad (eq. 2)$$

Where r is the rate of CH_4 production or growth, E_a is the activation energy of the reaction (in eV), k_B is the Boltzmann constant (8.617×10^{-5} eV K $^{-1}$), T is the temperature (in kelvin (K)) and

A is the pre exponential factor (a constant). It is also common to take the natural logarithm of the equation to obtain the equation in a form of a straight line:

$$\ln r(T) = -E_a \frac{1}{k_B T} + \ln A \quad (\text{eq. 3})$$

Where $\ln r$ is the natural logarithm of the reaction rate and $\ln A$ is the natural logarithm of the pre-exponential factor. For a reaction with rate that follows the Arrhenius equation a plot of $\ln r$ against T^{-1} will yield a straight line, where the activation energy of the reaction can be determined by the slope. The activation energy is the amount of energy required to initiate a certain reaction. If the activation energy changes over time, that is an indication that the rate limiting reaction of the system becomes a different one. When the overall effect of increased temperatures is increased catalytic rates, the metabolic rates of the organisms that expresses the enzymes are expected to increase as a result, and thus the rate of growth and formation of respiratory or fermentative end-products.

Gabriel Yvon-Durocher et al. (2014), showed in their study that many ecosystems and methanogenic isolates respond to increase in temperature in a way that can be predicted by the Arrhenius equation. Other studies have shown that this is not the case. Ratkowsky et al. (1983), showed that growth rates of microorganisms responded to temperature increases in a way that deviated from the Arrhenius equation (Ratkowsky, et al., 1983). Later, Tveit et al., showed that the temperature response of Arctic peat methanogenic systems also deviated from that predicted by the Arrhenius equation (Tveit, et al., 2015). The discrepancies observed may be explained by the consideration of different temperature ranges. Both Tveit et al. and Ratkowsky et al. (1983) considered temperature ranges spanning as much as 30 °C. There were speculations by Tveit et al. (2015) that adjustments in the gene expression and number of predatory protists grazing on prokaryotes and the lack of increases in the microbial biomass with increasing temperature were linked to the CH₄ production rate and thus its deviation from the Arrhenius prediction, but it was never understood how.

The data presented by Yvon-Durocher et al., contains multiple data points that deviate from their prediction as commented by Hoehler and Alperin (Hoehler & Alperin, 2014). For example, approximately 40% of the studies considered by Yvon-Durocher had Arrhenius plot correlation coefficients (r^2) of less than 0.5. This means that less than half of the variation in the data is explained by the Arrhenius equation, showing that the Arrhenius equation can predict

a large fraction of temperature dependencies in CH₄ producing microbial ecosystems, but far from all. A broad temperature range can account for some of the lacking explanatory power in the use of the Arrhenius equation as enzymes simply fail to function appropriately when the temperature becomes sufficiently high or low.

1.3.2 Effect of temperature on cells

Microorganisms can react to changes in temperature by changing a variety of cellular structures. As already described, temperature has significant effects on proteins, but membranes are also known to be influenced by temperature. Membranes can become more rigid or fluid due to larger proportions of saturated or unsaturated fatty acids as a response to higher or lower temperatures as cells cannot grow at temperatures below or above the solidification or melting point of the membrane (Marr & Ingraham, 1962). It was for instance shown that the expression of *desA* in Cyanobacteria, a gene encoding a desaturase which inserts double bonds to fatty acids, was increased 10-folds by decreasing the temperature from 36°C to 22°C (Los, et al., 1993).

DNA is very resilient to increases in temperature as PCR is evidence of. However, there are some strategies employed by prokaryotes living at very high temperatures to protect their DNA such as increased levels of cytoplasmic salts, novel polyamines (Terui, et al., 2005), positive supercoiling of the DNA (Los, 2004) and histone-like structures that weave the DNA into tight structures (Grosjean & Oshima, 2007). The replicational and transcriptional apparatus is probably more susceptible to temperature, such as DNA and RNA polymerase.

Ribosomes, the translational units of the cell, contain two components: the small and large ribosomal subunits (30S and 50S in prokaryotes, respectively) which are both composed of ribosomal RNA (rRNA) and multiple ribosomal proteins (Reuveni, et al., 2017). Ribosomes are important for the cells, and their abundance and efficiency have been seen to be closely associated with constraints on microbial growth (Scott, et al., 2014). The ratio of rRNA to protein in ribosomes can vary from between 20-70% rRNA (Reuveni, et al., 2017). It has been suggested that ribosome can change their composition in response to differences in environmental stimuli (Samir, et al., 2018) and as a mean of regulation of translation (Mauro & Matsuda, 2016). It has been shown that the rRNA of the thermophilic *Bacillus stearothermophilus* contains a higher quantity of cytosine and guanine compared to the rRNA

of *Escherichia coli* (Friedman, et al., 1967) and that the genes of r-proteins of an Antarctic ciliate had mutations that produced amino acids which caused increased structural flexibility (Pucciarelli, et al., 2005).

1.3.3 Temperature effects on microbial communities

Generally, there is a temperature range where each individual microorganism can sustain life. Different microbes will have different ranges, and generally the range narrows as one considers different modes of life from simply surviving, to growing, to reproducing. When the environment of the cells undergoes changes, there is usually a period of acclimatization where the organisms change physiological processes in response to the environmental change.

Although microorganisms respond individually to temperature changes, the effects on communities might be more severe because of the combined response of multiple members of the microbial community. In pairs of competitors one side might be more tolerable to temperature change and therefore outcompete the other side. Changes to organisms upstream in a decomposition chain could potentially lead to increased or decreased production of substrates for downstream microorganisms. There is evidently a complex dynamic present between members of a microbial community, and while the major temperature effects on chemical processes and microbial cells are well described, the effects of temperature on microbial communities are inconsistent and not well understood (Radujkovic, et al., 2018). Several studies have shown small or no changes in microbial communities as a result of temperature (Radujkovic, et al., 2018). However, some studies claim to have identified microbial groups that consistently respond to temperature changes in soil (Oliverio, et al., 2016). Very few studies have investigated the functional roles of microbial community members that respond to temperature changes. In Arctic peat soil from Svalbard it was shown that temperature increases led to few changes in the microbial community, but large changes in the transcriptional activity of the microorganisms, especially predatory protists and the syntrophic fermenters and methanogens at the end of the decomposition chain (Tveit, et al., 2015).

1.3.4 Community driven processes

As the effect of temperature on microbial communities are not well explained, the effect of changing microbial communities on the rates of CH₄ and CO₂ production are also poorly understood. Essentially, for temperature to alter a microbial community, temperature must have a disproportionately large effect on one or a few populations of microorganisms, enough for these organisms to either grow much faster or much slower than the other organisms in the ecosystem. Second, for these increasing or decreasing populations to make CH₄ or CO₂ production rates higher or lower than corresponding to the temperature effect on the chemical reactions their enzymes catalyze, their role in the ecosystem must be a role that becomes more or less important with temperature change.

1.4 Objective

The main goal of this master thesis is to look at how time plays a role in the effect of temperature on CH₄ production in Arctic peat soil. Secondly, we intended to identify the responses in the microbial community associated to the CH₄ production. The experiment was set up with a temperature gradient meant to simulate a natural increase in temperature from late spring to summer on Svalbard, with a high enough number of replicates and time-points to decipher the time-response in both CH₄ production and the microbial community. By using replicates originating from the same homogenous batch of soil slurry, we aimed to minimize heterogeneity in the soil that is unrelated to the questions asked.

1.5 Hypotheses

1. Being within a narrow temperature window, the temperature effect on CH₄ production is predicted by the Arrhenius equation at the end-point of incubation at all temperatures.
This hypothesis is derived from the results of Ratkowsky et al. (1982), Yvon-Durocher et al. (2014) and Tveit et al., (2015). These studies show that the temperature effect on CH₄ production and microbial growth rates can be predicted by the Arrhenius equation within narrow temperature ranges. Ratkowsky et al. and Tveit et al. showed that with extended temperature ranges, the Arrhenius equation loses its predictive ability.

2. Immediately after temperature change, the Arrhenius equation cannot predict the temperature effect on CH₄ production. *This hypothesis is derived from the biological adaptations observed in Tveit et al. (2015) and the unexplained variance in Yvon-Durocher et al. (2014).*
3. The community composition does not change as a result of temperature changes. *This hypothesis is derived from the lack of consistent changes observed in microbial communities exposed to temperature change (Radujkovic, et al., 2018) and the lack of community composition changes in Tveit et al. (2015). Nevertheless, we decided to test this hypothesis because the number of replicates is consistently low in most published studies tackling these issues, while the amount of soil heterogeneity is very high. Using samples from one homogenous batch of soil slurry and multiple replicates for each condition a new test of this hypothesis is justified.*

2 Materials and methods

2.1 Sampling and setup

The peat soil used in the experiment was sampled at Knudsenheia, Ny-Ålesund, Svalbard in August 2016. The soil was mixed in a 1:1 (w/w) ratio with water under anaerobic conditions and poured into a 1.5L stainless steel bottle and stored at 4°C until May 2017. The soil slurry was then moved to 2°C where it remained until the start of this experiment (April 2018). The bottle was shaken once per day for 30 seconds during the entire incubation period to achieve a homogenous microbial ecosystem.

From the soil slurry homogenate 42 ml was transferred into each of seventeen 120 ml headspace flasks. Two ml of slurry from each flask was transferred to 1.5 ml plastic tubes and frozen at -80°C, before the flasks were capped. The capped flasks were then flushed in 3 intervals with nitrogen to get rid of oxygen and carbon dioxide before starting the experiment. First flushing lasted for 5 minutes, directly after capping the flasks. Second flushing was 3 days later and was performed as 2 x 7 min. The last flushing was performed the same day as the first sampling, the day after the second flushing, and lasted for 3 min. Flushing in intervals was necessary to ensure that oxygen and CO₂ dissolved in the water would diffuse to the headspace to be removed in the later intervals.

The temperature incubation experiment was designed to simulate the natural increase in temperature on Svalbard from Spring into summer, with the highest temperature in the experiment being above the average past observations at the height of summer (figure 4).

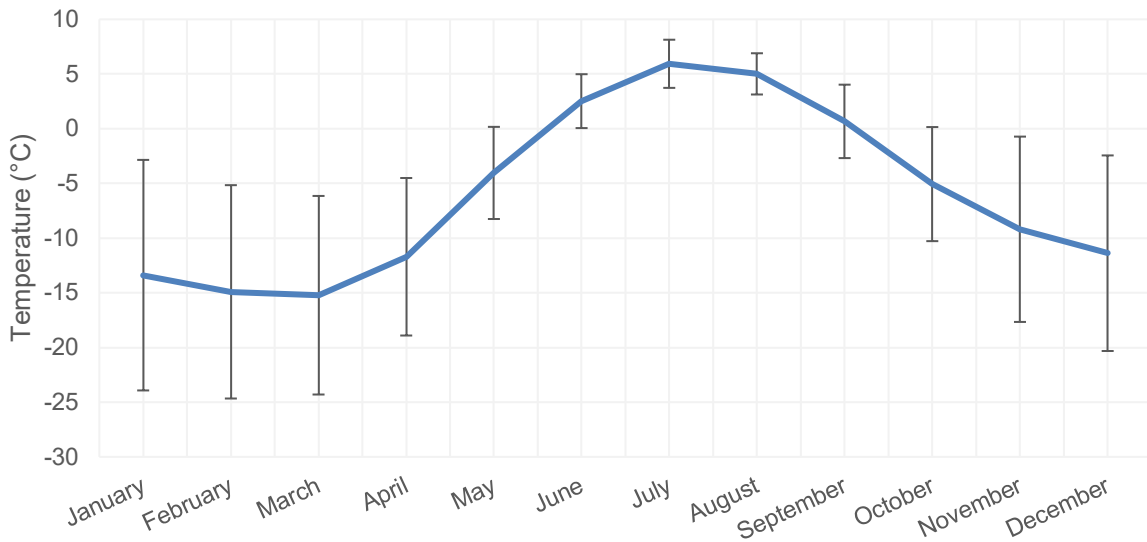


Figure 4 The average air temperature over a year at Svalbard and 2-standard deviation error bars indicating the variation within each month. Based on temperature data from Adventdalen over the last 120 years. © Metrological institute of Norway.

All 17 sample flasks were incubated at $\sim 2^{\circ}\text{C}$ for the 14 first days. Thereafter, 13 of the flasks were moved to a higher temperature ($\sim 3^{\circ}\text{C}$), while 4 randomly (selected using the list randomizer at www.random.org) chosen flasks were left at 2°C . The 13 flasks remained at $\sim 3^{\circ}\text{C}$ for 7 days and was then moved to $\sim 5^{\circ}\text{C}$ where they remained for 6 days. After this period 9 of the flasks were moved to incubation at $\sim 7.5^{\circ}\text{C}$, while 4 randomly selected flasks remained at 5°C . After 7 days at 7.5°C the flasks were moved to 9°C . Nine flasks were then at 9°C , four at 5°C and four at 2°C until the end of the experiment which was 53 days after the first sampling began. The position of the flasks in the incubators were shifted after each sampling to avoid biases based on localization within the incubator.

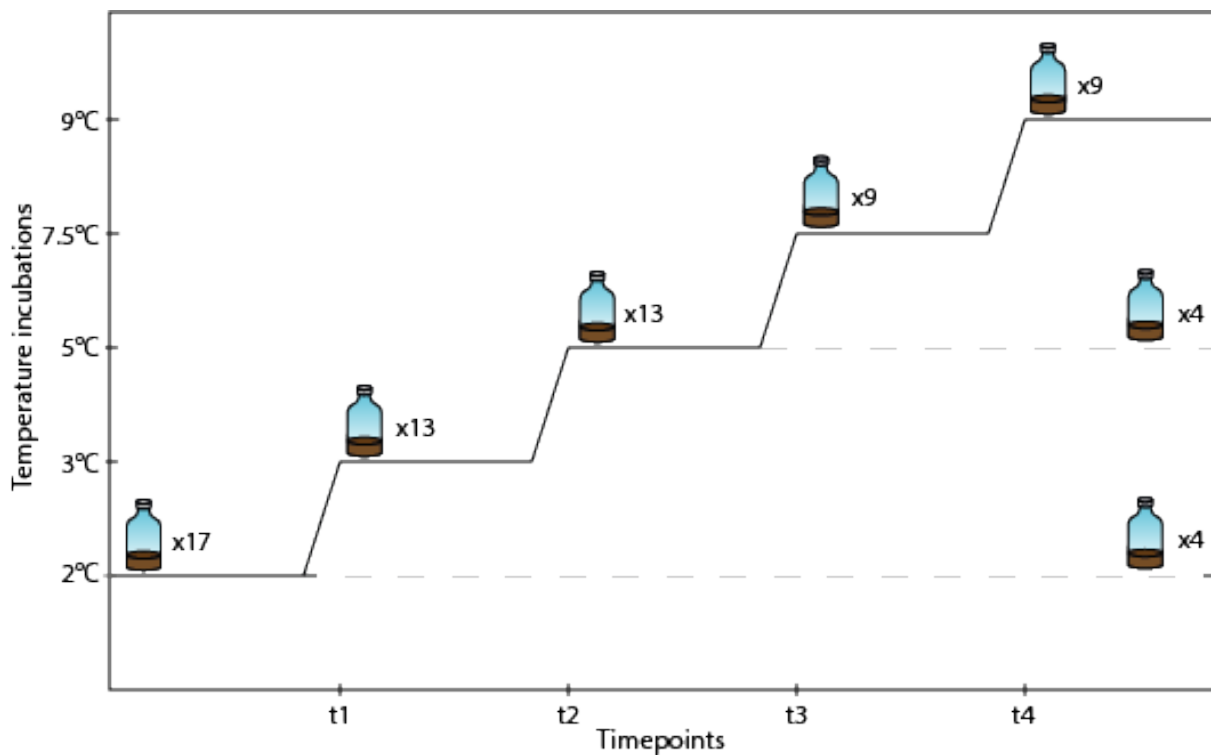


Figure 5 Schematic overview of the experimental setup of the temperature incubations.

2.2 Gas sampling and measurement

Gas samples were collected from all seventeen sample flasks approximately 4 times per week of the incubation for the measurement of CO₂ and CH₄ concentrations. Twenty-nine exetainer vials with caps containing septa were prepared each time. One per sample for a total of 17, six for the standards containing 0.1% CH₄ and 0.2% CO₂, and six for the standards containing 1% CH₄ and 1% CO₂. Air was drawn from each exetainer for 30 secs using Edwards KNF Neuberger vacuum pumps. The exetainers were then flushed with nitrogen (N₂) for 30 secs and subsequently pierced with a needle to release any overpressure.

The VICI Pressure-Lok® Precision analytical syringe was used to obtain the gas samples from the sample flasks as well as the standards. For the two sets of standards (0.1% CH₄ + 0.2% CO₂ and 1% CH₄ + 1% CO₂), the syringe was first flushed three times with N₂ (99.999% purity, Alphagaz™ 1 Stickstoff, Air Liquide Austria GmbH. A volume of 0.25 ml of standard gas was extracted with the empty syringe. These 0.25 ml were injected into a “standard” exetainer. This was done for 6 standard exetainers without flushing in between. Before the next set of standards, the syringe was flushed again three times with N₂ before repeating the same procedure.

For the samples, the syringe was flushed three times with N₂ (99.999% purity, Alphagaz™ 1 Stickstoff, Air Liquide Austria GmbH). Then, 0.25 ml of N₂ was drawn into the syringe. Pressure was released from the syringe by opening the valve. The sample flask was shaken, and the syringe was pierced through the septum of the sample flask. The nitrogen content of the syringe was expelled into the flask to avoid changes in gas pressure, and 0.25 ml sample was extracted. The sample was then injected into the respective extainer. This flushing and sampling procedure was repeated for each of the 17 sample flasks. The samples were then analyzed on a gas chromatograph TRACE GC Ultra with a Flame Ionization Detector (FID) from Thermo Scientific.

A new gas extraction syringe was used as of day 27 because of problems with the original syringe between day 21 and 26, which led to faulty measurements during these days.

2.3 Determination of microbial growth

Estimation of growth was performed at the department of Terrestrial Ecosystem Research at the University of Vienna according to the ¹⁸O incorporation method as used in (Walker, et al., 2018) which allows for estimations of average microbial growth rate based on the amount of ¹⁸O incorporated into microbial DNA from H₂¹⁸O. This was performed on the last day of the incubation period on the same samples as for the enzyme assays. Water content of the soil was calculated from the drying at 100°C for 24 h of 2 grams of wet soil slurry. The water content of the soil was used for calculations of the ¹⁸O enrichment in the soil water later.

Three hundred and fifty mg of soil was weighed into two sets of 1.2 ml Semadeni cryovials for every sample, one set for the determination of the natural abundance of ¹⁸O (control) and one for the enrichment. The vials were confined in airtight headspace vials. A volume of 145 µl Mol. Bio grade water was added to the control samples, and 145 µl ¹⁸O water was added to the enrichment samples. A gas sample was taken at t₀ and the vials were then flushed to get rid of CO₂. All vials were incubated at their respective temperatures (2, 5 and 9°C) for 24 h to 48 h. After incubation a new gas sample was collected for every sample. The headspace vials were opened, and the cryovials were quickly closed and frozen in liquid N₂.

DNA was extracted from the samples using the MP Bio DNA Fast Spin Kit (MP Biomedicals) as according to the protocol of appendix I.A. The DNA was then quantified specifically for the

¹⁸O experiment with PicoGreen (Quanti-iT™ PicoGreen, Life Technologies). DNA extracts were diluted in 1X Tris-EDTA (TE) buffer and 100 µl pipetted in a black microtiter plate, along with prepared DNA standards and blanks. One hundred µl PicoGreen reagent diluted in 1X TE was added to samples, standards and blanks. The plate was incubated at room temperature for 5 min and fluorescence was measured at excitation 480 nm and emission 520 nm. Full protocol can be seen in appendix I.B.

2.4 Extracellular enzyme assays

Extracellular enzyme activity was measured by the department of Terrestrial Ecosystem Research at the University of Vienna at the end of the incubation period. The enzymatic activity of the hydrolytic, extracellular enzymes betaglucosidase and leucine aminopeptidase (protease) in the four 2°C samples, the four 5°C control samples and four randomly chosen samples of the 9°C treatment (samples 1, 5, 9 and 13) was determined using microplate fluorometric assays. Two grams of peat soil slurry was suspended in 50 ml Na-acetate buffer (50 mM, pH 6.5) and sonicated for some seconds to reach an energy output of 350 J. Subsequently, 200 µl of the soil suspension and 50 µl substrate (4-Methylumbelliferyl-β-D-glucopyranoside and L-leucine-7-amido-4-methylcoumarine, respectively) were pipetted into black microtiter plates in 5 technical replicates. Methylumbelliferyl (MUF) was used as a standard for the betaglucosidase while aminomethylcoumarin (AMC) was used to calibrate protease activity. All plates were incubated at 6°C for 15 min in the dark and measured at 365 nm excitation and 450 nm emission (using a Tecan Infinite M200fluorimeter, Werfen, Austria) every 30 minutes for 7 time points with incubation at 6°C between every measurement. Measuring at the same temperature ensures that the activity is dependent only on the number of enzymes accumulated through incubation and not the thermokinetic effect in addition. Extracellular enzyme activities were calculated using the increase in fluorescence over time, corrected for the amount of soil that was weighed in and expressed in [nmol g⁻¹ DW h⁻¹].

2.5 Determination of microbial community compositions

2.5.1 Sample preparation

Samples were prepared for extraction by soil grinding. There were two sets of 17 samples taken from the 17 flasks at the start (S1-S17) and end (E1-E17) of the experiment. The sample tubes were carefully broken with a pestle in a cooled down mortar. Plastic pieces were removed, and the soil was grinded through 4 rounds of liquid nitrogen addition, until reaching a fine powder. Approximately 0.2 g of soil from each sample was transferred to each of two pre-weighed lysis matrix E tubes. The tubes were weighed again for precise determination of soil weight, before being stored at -80°C. All equipment was washed with soap and rinsed with water followed by a rinse with 70% ethanol between each round of grinding a new sample.

2.5.2 Total nucleic acid extraction

Total nucleic acids were extracted with a phenol-chloroform protocol (Tveit, et al., 2013). Five hundred μ l extraction buffer (5% Cetyl Trimethylammonium bromide (CTAB)/ 120 mM K₂HPO₄, pH 8) was added to the lysis matrix E tubes, along with 500 μ l Phenol Chloroform Isoamylalchohol (PCI, 25:24:1). The tubes were bead beating at 5.0 for 30 seconds followed by centrifugation at 13000 g, 4°C for 10 min. Five hundred and fifty μ l supernatant was transferred to a 2 ml tube. One volume (550 μ l) of Chloroform Isoamylalchohol (CI 24:1) was added and mixed with supernatant by turning the tube a couple of times. The tubes were centrifuged for 5 min at 13000 g and 4°C. The top phase supernatant (550 μ l) was transferred to a new 2 ml tube. A volume of 5.4 μ l glycogen (5 mg/ml) was pipetted into the supernatant, after which 2 volumes (1.10 ml) of PEG-6000 (polyethylene glycol) was added. The content of the tube was mixed by flipping once, carefully, and left to precipitate on ice for 60 min.

After precipitation the samples were centrifuged at 13000 g, 4°C for 60 min for a pellet to form. The supernatant was decanted in those cases where the pellet was firmly attached to the side of the tube or pipetted if pellet was loose. One ml of 70% ice cold ethanol (EtOH) was added, and the samples were centrifuge for 10 min at 13000 g and 4°C. Decanting of supernatant and EtOH wash was performed once more. The tubes were spun down for 5 sec to collect remaining EtOH which was removed by careful pipetting. The pellet was then dried in an Eppendorf

Thermomixer R at 50°C for 1-2 min. The pellets were eluted in 50 µl DEPC treated water and 0.5 µl RNase inhibitor (RiboLock (40 U/, ThermoFisher Scientific) was added. Purity and concentration were measured using NanoDrop 1000 (ThermoFisher Scientific) before being stored at -80°C.

2.5.3 DNA quantification and quality check

Quantification of the amount of DNA in the samples were performed on the Qubit® 2.0 Fluorometer (ThermoFisher Scientific) with the Qubit® DNA dsDNA HS Assay Kit . First, 200 µl of working solution per sample and standard (to a total of 7.2 ml) was prepared by diluting the Qubit™ reagent 1:200 in Qubit™ buffer. A volume of 190 µl working solution was distributed to the thin-walled, clear 0.5 ml Assay tubes for the standards, and 10 µl of standard 1 and 2 were added, respectively, for a total volume of 200 µl per tube. For the sample tubes, 199 µl working solution was added. A volume of 1 µl of sample was then added to the respective tubes, for a total volume of 200 µl per tube. All tubes were vortexed for 2 sec before being incubated at room temperature for 2 min. The two standards were firstly measured for calibration of the Qubit Fluorometer. The DNA concentration of the samples were then measured and calculated back to the stock concentration by the Qubit.

Two 1% agarose gel were produced for quality check of the DNA from the replicates. A volume of 1 µl of the samples were mixed with 1 µl of 6X MassRuler™ DNA Loading Dye (Thermo Scientific) and 4 µl H₂O. The total volume of 6 µl was loaded onto the gel along with 3 µl of the FastRuler™ Low Range DNA Ladder (Thermo Scientific) All samples contained visible DNA bands, except for the first replicate of sample S1 which had a smear (appendix I.C). This sample was therefore excluded from the sequencing.

2.5.4 16S amplicon sequencing

Untreated samples of total nucleic acids were sent to IMGM Laboratories GmbH (Martinsried, Germany) for amplicon sequencing. PCR was performed on all samples using a specific primer set for bacterial and archaeal 16S rRNA genes (table 1). This primer set was chosen because of its high coverage towards both Bacteria and Archaea. Detection for candidate divisions WS6, OP11, TM7 and OD1 is unlikely and can be low for *Chlamydiae*, *Calidserica*, *Chloroflexi*, SM2F11, Lazan-3B-28 and BHI80-139, and for the Archaea the phyla AA, MHVG-1, MHVG-

2 and *Nanoarchaeota* can also be hard to detect (Klindworth, et al., 2013). For percentage coverage of the primers refer to appendix I.D. Barcodes for multiplexed sequencing were introduced during index PCR using overhang tags. One amplicon library was prepared from the barcoded PCR products.

Table 1 16S rRNA gene primer set used in PCR of samples.

Primer name	Position	Primer sequence	Region	Amplicon size (bp)	Reference
A519F	519-533	5'- CAG CMG CCG CGG TAA -3'	V4	Ca. 287	(Klindworth, et al., 2013)
Bakt_805R	785-805	5'- GAC TAC HVG GGT ATC TAA TCC -3'			

The sequencing was performed on the Illumina MiSeq® next generation sequencing system (Illumina Inc.). Signals were processed to *.fastq files and the resulting 2×250 bp reads were demultiplexed and quality controlled using CLC Genomics Workbench 12.0. Raw *.fastq files were provided from the sequencing facilities.

2.5.5 Data analysis

2.5.5.1 Sequence analysis

The provided raw *.fastq forward and reverse files were treated with a bioinformatics pipeline for amplicon sequences (Kalenitchenko, 2018). The files were imported into the QIIME2 microbiome analysis software (Boylen & al., 2018). In qiime DADA2 denoise-paired the forward and reverse sequences were trimmed to remove primers with 15 bp in the forward and 21 bp in the reverse and truncated to remove 5 bp and be left with 245 bp sequences. Reads with higher a number of expected errors than 1 was discarded. The forward and reverse reads were merged, and quality filtered with vsearch (Rognes, et al., 2018). Samples were concatenated with the mothur package (Schloss, et al., 2009) and then dereplicated and sorted by size with vsearch. OTUs were clustered at 97% with usearch (Edgar, 2010) and checked for chimeras. Taxonomy was assigned using the mothur package, and an OTU table was constructed with ‘biom()’.

2.5.5.2 Statistics and calculations

All regressions and plots were generated using excel and the ‘ggplot2’ package (Wickham, 2016) within the R Statistical Computing Platform version 3.5.2 and version 3.6.0 (R Core Team, 2018). Visualization of abundances by bar plotting was performed using the ‘phyloseq’ package (McMurdie & Holmes, 2013) and its ‘ggplot2’ extension.

Calculation of gas concentrations

The raw data of the gas (CO_2 and CH_4) measurements were provided as ppm and had to be converted to $\mu\text{mol}/\text{ml}$. Firstly, data points with large drops in concentrations (outliers) were removed. This included all sampled concentrations for day 21, 22, 23 and 26. Calculations of the total amount of gas in the headspace of the flasks were then conducted using the formula:

$$x \mu\text{mol gas in headspace} = \frac{(P_{t0} \times V) \times 4 \times 78 \times 10^6}{(T \times R) \frac{\text{ppm}}{10^6}} \quad (\text{eq. 4})$$

Where P_{t0} is the atmospheric pressure of the day the flasks were closed (in atm), V is the volume of the gas extraction syringe (0.00025 L), R is the gas constant (0.082057 L atm K^{-1} mol^{-1}), T is the temperature (in kelvin (K)) and ppm is the measured gas concentrations (in parts per million). Ppm is divided by 10^6 to get parts per 1. The equation is multiplied with 4 to get mol/ml. 78 to get mol/headspace and 10^6 to get $\mu\text{mol}/\text{headspace}$. The amount of gas was then adjusted for the proportion of gas that was removed for each gas extraction. As the total volume of the headspace was 78 ml, the 0.25 ml which was removed each time constituted 1/312 part of the volume. Then, the amount of gas that was dissolved in the liquid phase of the flasks were calculated as:

$$x \mu\text{mol gas in liquid} = \frac{\text{ppm}}{10^6} \times P_{t0} \times \frac{k_h(T)}{10^3} \times V \times 10^6 \quad (\text{eq. 5})$$

Where ppm is the measured gas concentrations (in parts per million), P_{t0} is the atmospheric pressure at the time the flasks were closed (in atm), V is the volume of the liquid phase (42 ml) and $k_h(T)$ is the temperature dependent solubility constant for the respective gases CH_4 and CO_2 (in mol L^{-1}). The ppm gas concentration was divided by 10^6 to get parts per 1. The solubility constant divided by 10^3 for mol per ml and multiplied with 10^6 to get $\mu\text{mol}/\text{liquid}$. Finally, the

sum was taken of the amount of gas in the liquid phase and the headspace and divided by the ml of slurry to get the μmol of gas per ml slurry.

Arrhenius calculation

Quantification of the temperature dependency of CH_4 production was calculated using the Boltzmann-Arrhenius equation as indicated by Yvon-Durocher et al. (2014) in the form given in **equation 3** in the introduction (1.3.1.1 The Arrhenius equation). The rate was calculated as the slope of linear regressions fitted for the CH_4 concentrations and the growth rates measured at each temperature. When assessing the rates at each temperature window, it was clear that for the 5 °C, 7.5 °C and 9 °C the rates were biphasic (appendix II.B). For each temperature the CH_4 production rates therefore split into two periods; ‘beginning’ meaning right after temperature change and ‘acclimatized’ which was at the end of the temperature window. This was done visually except for the 3 °C which lacked enough time points for a good resolution and for the 2 °C which were already considered to be acclimatized after being incubated for 2 years at the respective temperature. The average temperature for each incubation was transformed to the kelvin scale and multiplied with the Boltzmann constant. Three plots of $\ln r$ versus $k_B T^{-1}$ was made for the CH_4 production, one with both ‘beginning’ and ‘acclimatized’ production rates, one with only the ‘acclimatized’ rates and one with the ‘beginning’ rates. A plot of $\ln r$ versus $k_B T^{-1}$ was also produced for the growth rates. A linear regression model was fitted for each case, as well as polynomials for the ‘beginning’ samples of the CH_4 production and the growth rates. The activation energy (E_a) was found by multiplying the slope of the linear regression (can be calculated by $\Delta y/\Delta x$) with -1.

Significance tests

Welch Two Sample t-test were performed with the `t.test()` function within core R to test for significant differences in means of the amount of TNA between start and end samples. One-way ANOVA tests were used to test for significant differences in means where there were more than 2 groups. The ANOVAs were performed with the `aov()` function of core R to compare the TNA amounts between the different temperature treated end samples, to assess the difference in enzyme activity between the 3 different temperature treatments. To verify that the assumption of ANOVA of equal variance was satisfied a Levene’s test was performed before any ANOVA, using the `LeveneTest()` function under the ‘car’ package in R.

Correspondence analysis (CA)

A correspondence analysis (CA) was performed on the OTU table obtained from the bioinformatic processing. CA was applied because it grants a larger impact of low-abundance variables in the analysis than alternative methods. First, preparation steps of the OTU table was conducted. This included computing a proportion matrix from the OTU table, making vectors from the totals of the rows and columns, and making the square root of the vectors into diagonal matrices using the ‘diag()’ function of R. The matrices were then multiplied using the %*% operator. The Singular Value Decomposition (SVD) was computed with the ‘svd()’ function, and the principal and standard coordinates were calculated using the %*% operator. The inertia of the table was calculated and lastly, the coordinates could be plotted to generate the graphical representation of the CA analysis.

3 Results

3.1 Chemical

3.1.1 Temperature log

The initial temperatures of the incubations were meant to be 2°C, 4°C, 6°C, 8°C and 10°C to simulate a natural temperature increase at Svalbard during the transition from spring to summer. The temperatures of the incubation chambers were logged, and the real temperature of the chambers and the fluctuations are visualized in figure 6.

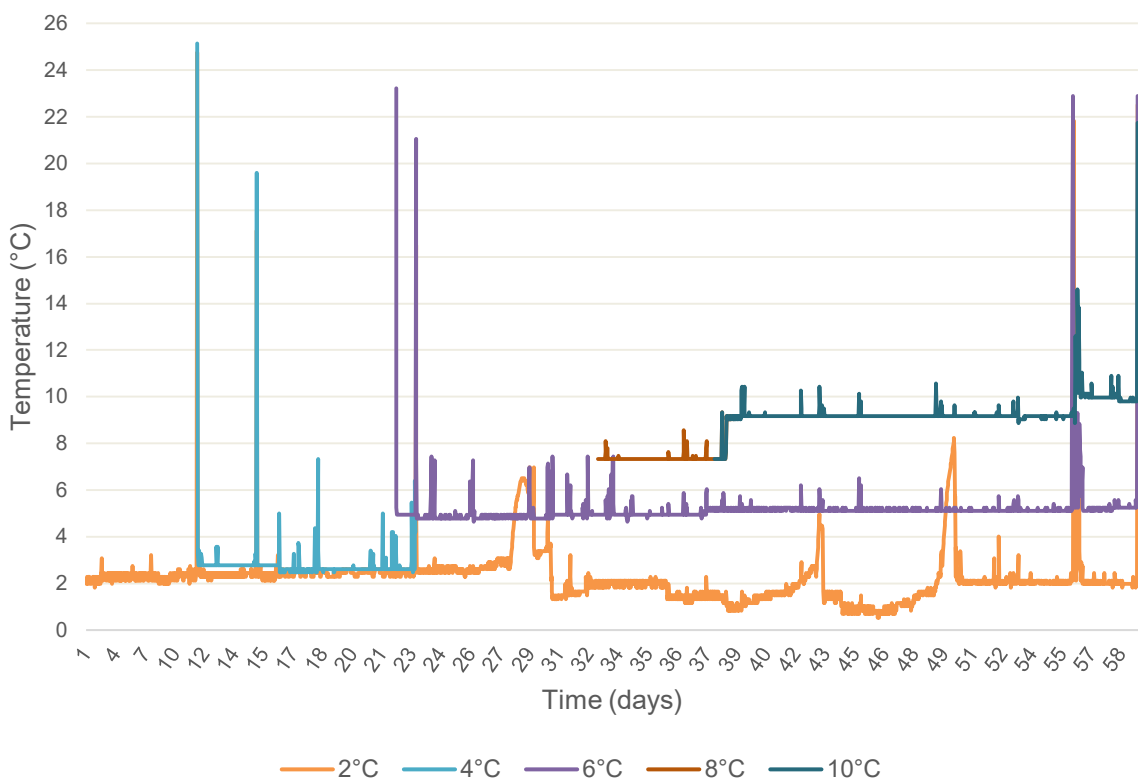


Figure 6 Results of the temperature logging showing the real temperature and fluctuations for the incubations. Orange line shows the fluctuation in temperature of the 2°C incubations, cyan line shows fluctuation of 4°C incubation, purple line shows fluctuation at 6°C, dark red shows fluctuation at 8°C and dark blue shows fluctuation at 10°C.

For the 2°C incubation the average temperature was 2.25°C, for the 4°C incubation the average was 2.82°C, for the 6°C the average temperature was 5.16°C, for the 8°C the average was

7.45°C and for the 10°C the average temperature was 9.29°C. Hereafter, the incubation temperatures will be named as 2°C, 3°C, 5°C, 7.5°C and 9°C.

3.1.2 Soil water content and pH

Drying of the soil and pH measurements at the end of the incubation period showed that the soil samples had high water contents ranging between 93.3% and 90.2% with an average of 91.9%. The pH of the samples was slightly acidic and ranged between 6.47 and 6.25, with an average of 6.32. Organic content was not measured as it is assumed to remain constant as all samples originate from the same homogenous soil slurry.

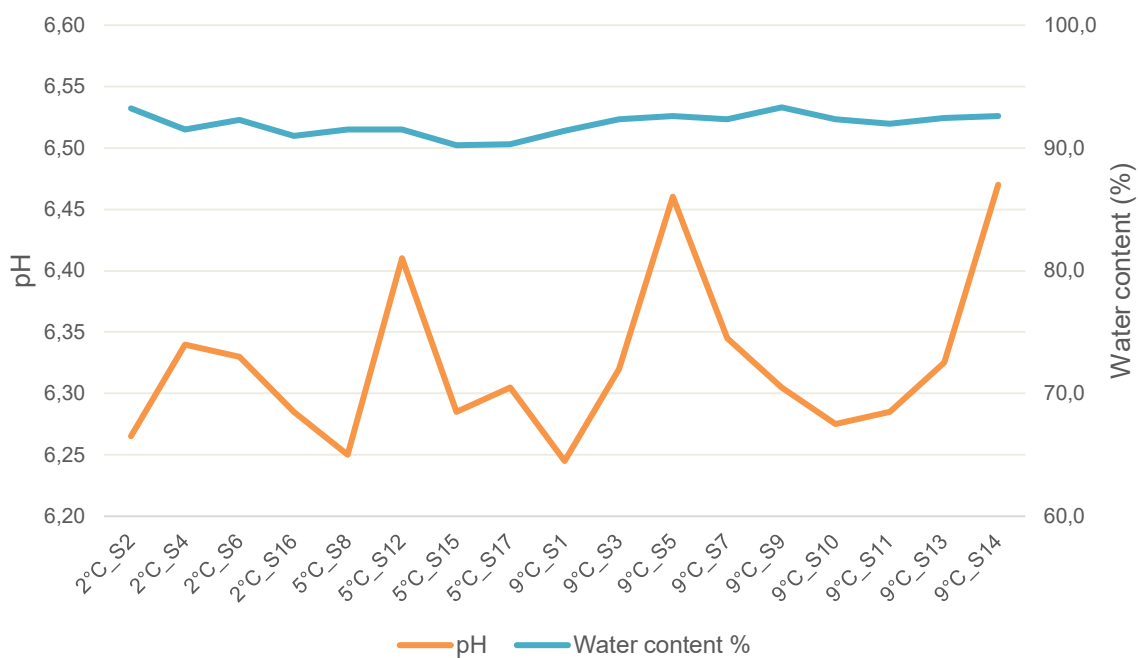


Figure 7 Variation of water content (%) and pH in samples 1 to 17 at the end of incubation, sorted after which temperature treatment they received.

3.1.3 CH₄ and CO₂ production

The monitoring of the CH₄ accumulation rate started the 17.04.18 after all 17 slurry flasks had been flushed with N₂. All flasks remained at 2°C for the initial 14 days of incubation. During this time, the CH₄ accumulation rates of all flasks followed the same trend (figure 8). At day 15, 13 bottles were moved to 3°C. During the seven days at 3°C, there were no signs that the CH₄ accumulation rate of these flasks deviated from those left at 2°C. At day 22 the flasks at

3°C were moved up to 5°C . Differences in the rate of CH_4 accumulation between the 2°C control samples and those that had been moved to 5°C were noticeable immediately after increasing the temperature from 3°C to 5°C . After 30 days of incubation, nine samples were moved up to 7.5°C , while four where left at 5°C as controls. The CH_4 accumulation rate then increased immediately, compared to the samples that had been left at 5°C . The same was observed after moving the samples from 7.5°C to 9°C . The production rates inferred from the slope of the linear regressions at the different temperatures (appendix II.A) were $0.0005 \mu\text{mol ml}^{-1} \text{d}^{-1}$ for the 2°C , $0.0006 \mu\text{mol ml}^{-1} \text{d}^{-1}$ for the 3°C , $0.0007 \mu\text{mol ml}^{-1} \text{d}^{-1}$ for the 5°C , $0.0007 \mu\text{mol ml}^{-1} \text{d}^{-1}$ for the 7.5°C and $0.0016 \mu\text{mol ml}^{-1} \text{d}^{-1}$ for the 9°C incubations. The linear rates of production of the 5°C and the 7.5°C does not correspond to the trend indicated in the floating regression (figure 8).

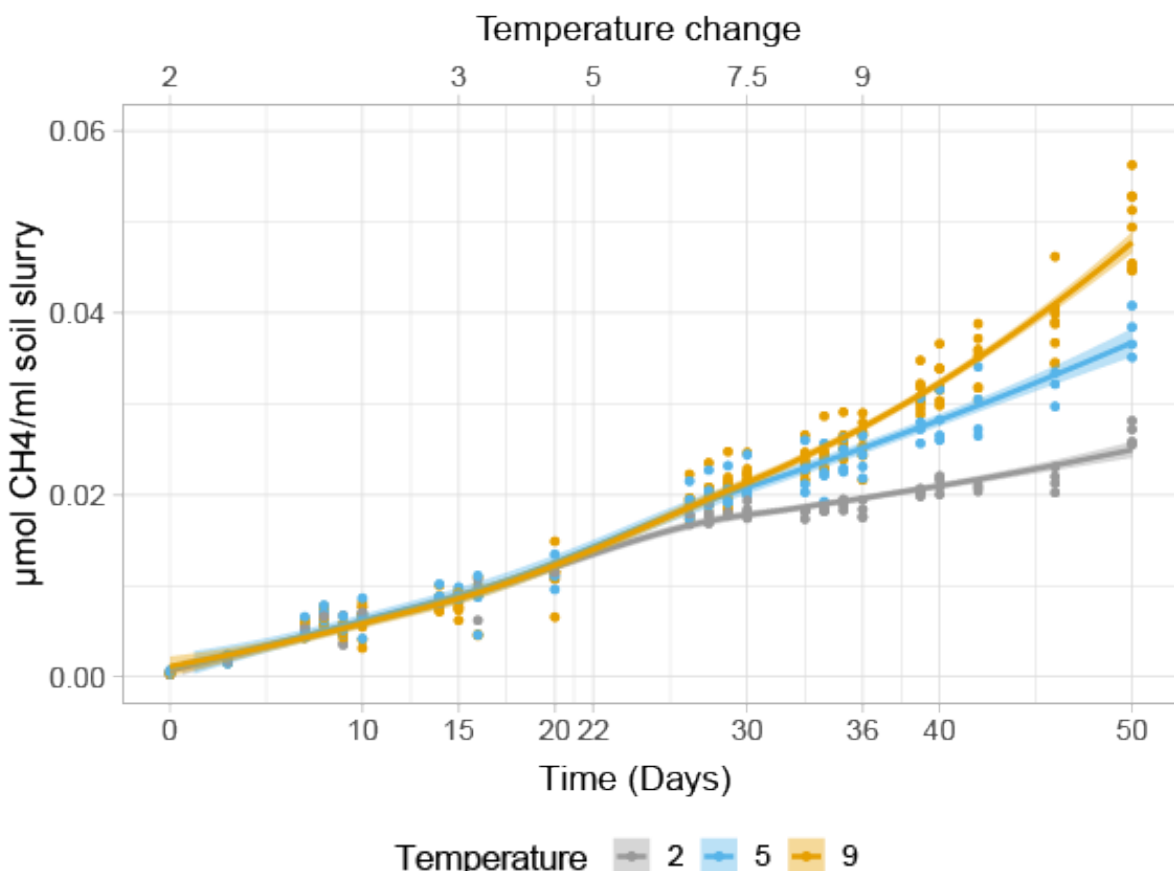
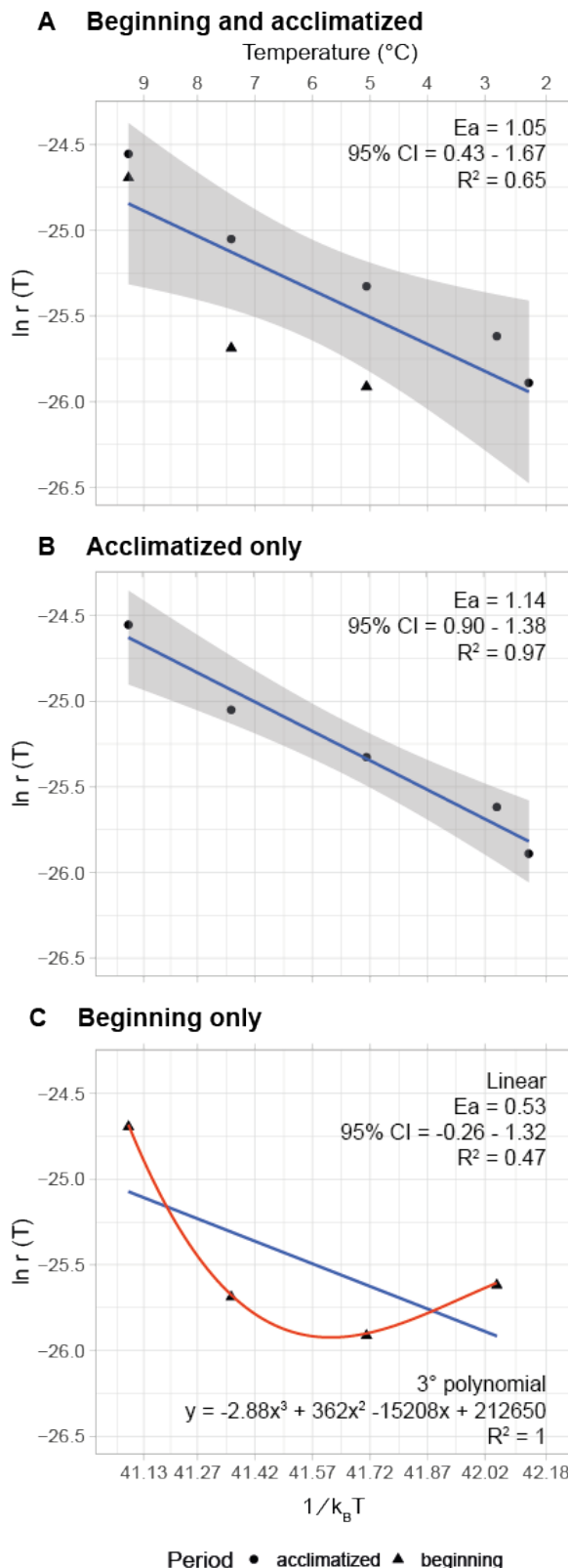


Figure 8 Concentration of CH_4 (μmol per ml soil slurry) as a function of time (days) with 95% confidence intervals. Data points are shown for all samples with a loess regression fitted and 95% confidence interval bands. Marked as grey are samples that remained at 2°C throughout the incubation, blue are samples that were changed from 2°C to 3°C at 15 days after incubation start and lastly to 5°C on day 22. The samples that were moved through all temperature incubations, from 2°C to 3°C after 15 days, to 5°C after 22 days, 7.5°C after 30 days and finally to 9°C , are marked in orange.



The temperature dependence of reaction rates can be calculated using the Arrhenius equation. Here we assessed whether the observed temperature effects on CH₄ production follows the Arrhenius equation (figure 9). For each temperature window the CH₄ production rates were split into two periods (appendix II.B); ‘beginning’ meaning right after change in temperature and ‘acclimatized’ which were at the end of the temperature window. The analysis with ‘beginning’ and ‘acclimatized’ values combined indicated a temperature dependence of CH₄ production by an activation energy (E_a) of 1.05 eV (The slope of the linear model fitted to the Arrhenius plot) with a 95% CI of 0.43 – 1.67 eV (figure 9.A) and R² of 0.65. The ‘beginning’ data points for the 5°C and 7.5°C lies outside the 95% CI.

Removal of the ‘beginning’ rates for the 5-, 7.5- and 9°C incubations improved the fit of the data points to the linear regression model considerably with an R² of 0.97 (figure 9.B). A linear regression analysis for the ‘beginning’ samples only gave an estimate of the temperature dependence of 0.53 with a 95% CI of -0.26 – 1.32. The linear regression had an R² of 0.47. A 3rd degree polynomial was better suited to explain the variation with an R² of 1

Figure 9 Arrhenius plot of (A) rates divided into beginning and acclimatized points (except for 2°C and 3°C) against 1/k_BT with a linear regression with slope 1.05 and a 95% CI shown in grey of [0.43-1.67], (B) ‘beginning’ points have been removed which resulted in a slope of 1.14, and a tighter 95% CI of [0.90-1.38] and (C) only beginning points with a linear regression (blue line) with slope 0.53 and a 95% of [-0.26 – 1.32] and a 3rd degree polynomial (red line) to show a better fitted regression model. The 3°C was included in all three plots.

(figure 9.C), suggesting that microbial acclimatization to temperature shifts were more pronounced in the 5 and 7.5°C temperature shifts than in the shift to 9°C. Too few data points existed for the 3°C shift to allow a split into ‘beginning’ and ‘acclimatized’ values, while no shift existed from a lower temperature to 2°C. Thus, these data points were ignored as such.

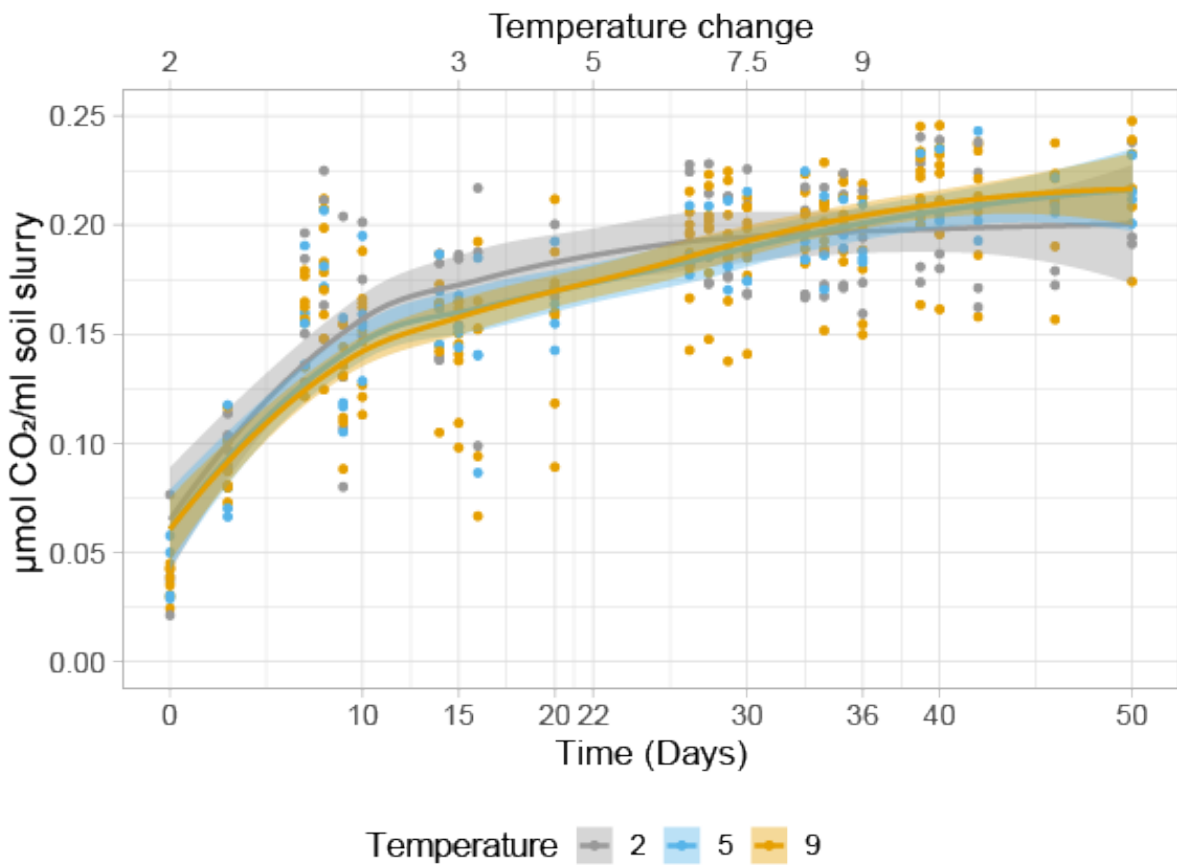


Figure 10 Concentration of CO₂ (μmol per g dry soil) as a function of time (days) with 95% CI bands. Data points are shown for all samples with a loess regression fitted and 95% confidence interval bands. Marked as grey are samples that remained at 2°C throughout the incubation, blue are samples that were changed from 2°C to 3°C at 15 days after incubation start and lastly to 5°C on day 22. The samples that were moved through all temperature incubations, from 2°C to 3°C after 15 days, to 5°C after 22 days, 7.5°C after 30 days and finally to 9°C, are marked in orange.

The CO₂ measurements from all 3 temperature treatments have curves that resemble a saturation curve with a higher production rate at the start of the experiment, and then decreasing rates until the concentrations almost becomes constant, however, not completely. The treatments have very similar trends for the CO₂ concentrations with overlapping 95% CI along the whole time series (figure 10). From day 0 until the 7.5°C were moved to 9°C at day 30, all

samples show the same trend in CO₂ concentration, even though the rest of the samples were separated from the 2°C control samples at day 15 and had been moved from 3°C to 5°C. After day 30 the samples separate more. The 9°C samples shows higher CO₂ concentration than the 2°C controls but has overlapping 95% CI with the 5°C control samples. The 5°C and 2°C controls have overlapping 95% CI, signifying a non-statistical difference between these samples.

3.1.4 Mass specific growth

To measure the growth rates of the microbiome an ¹⁸O incorporation experiment where the amount of ¹⁸O stable isotope incorporation into DNA from water enriched in ¹⁸O (H₂¹⁸O) was performed. A one-way ANOVA showed there was a significant difference among the 2-, 5- and 9°C samples ($F(2,9) = 21.5$, $p = 0.0003$). Post hoc comparison using the Tukey's pairwise indicated that the 9°C samples had significantly higher mass specific growth rate compared to the 5°C samples ($p = 0.001$) and the 2°C samples ($p = 0.0005$). However, the 2°C and 5°C did not significantly differ from each other (figure 11).

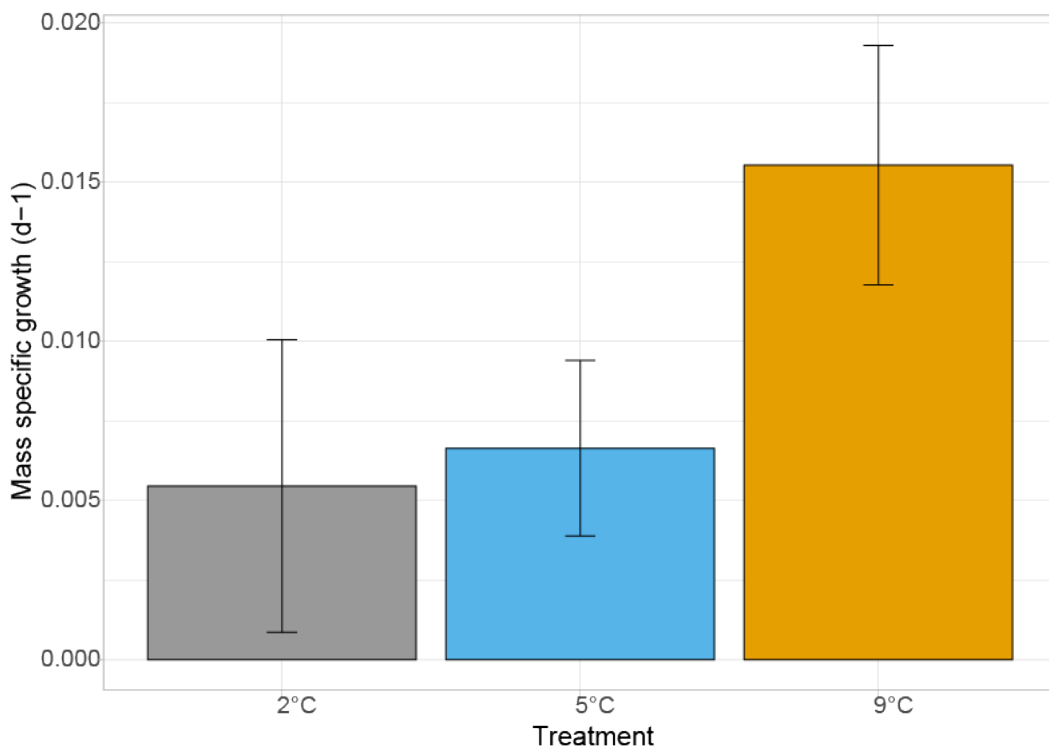


Figure 11 Mass specific growth with 95% CI bars for the 2°C, 5 °C and 9 °C treatments. A Levene's test showed no homogeneity of the sample variances ($p = 0.57$).

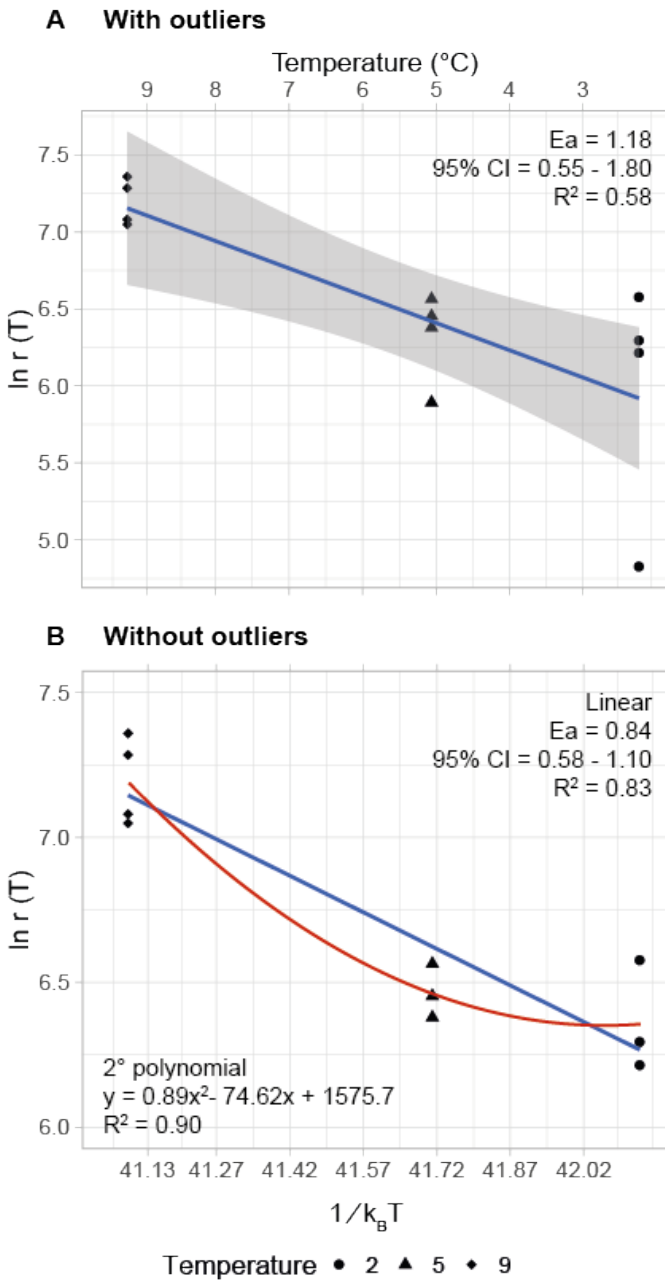


Figure 12 Arrhenius plot of (A) growth rates with outliers and a linear regression fitted with a 95% CI marked in grey, and (B) growth rates without outliers showing a linear regression (blue line) and a better fitting 2nd degree polynomial.

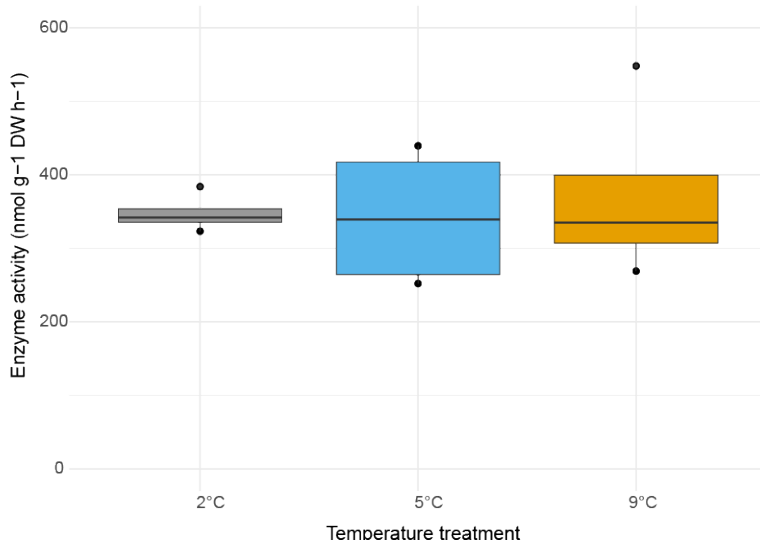
Similarly, as for the CH₄ production rates, we tested whether or not the temperature dependence of the growth rates could be predicted by the Arrhenius equation. The temperature dependence of growth reflected an Ea of 1.18 eV with a 95% CI of 0.56 – 1.80 and R² of 0.58 (figure 12.A). It can be seen in the plot that two lower outliers from the 2°C and 5°C incubations contribute to lowering the prediction from the linear model. Removing the outliers makes the linear model has a poor fit for the data. Replacing this with a 2nd degree polynomial model substantially improves the fit with an R² of 0.90 (figure 12.B), suggesting that the growth of the microorganisms cannot be predicted by the Arrhenius equation.

3.1.5 Enzyme activity

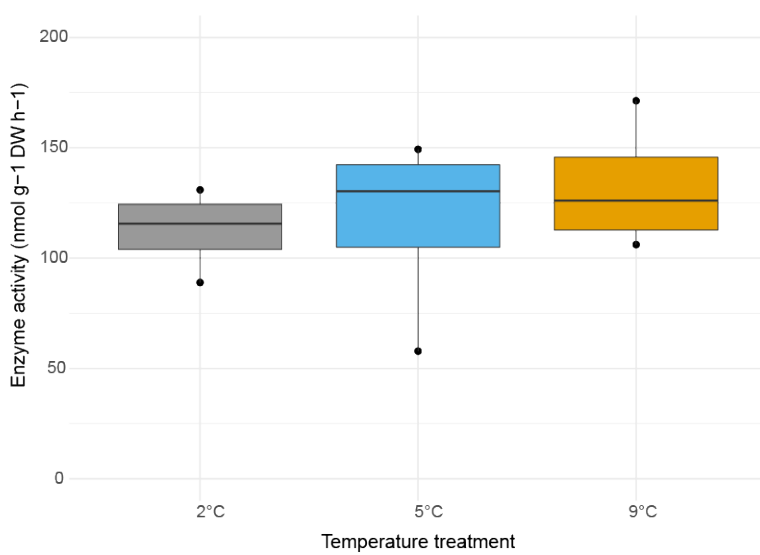
Potential enzyme activities of beta-glucosidase and leucine aminopeptidase was measured at the end of the incubation period for the evaluation of the temperature effect on microbial investment into extracellular decomposition of oligosaccharides and peptides. Activity was measured at 6°C, thus making sure that it is the number of enzymes that is measured, not the combination of the thermokinetic effect and the number of enzymes. The activity of beta-

glucosidase (figure 13.A) was higher than the activity of leucine-aminopeptidase (figure 13.B). For the beta-glucosidase the activity was around $300 \text{ nmol g}^{-1}\text{DW h}^{-1}$, and around $125 \text{ nmol g}^{-1}\text{DW h}^{-1}$ for the leucine-aminopeptidase.

A β - glucosidase



B Leucine - aminopeptidase



A one-way ANOVA to test for significant differences in activity was conducted for the three temperature treatments of the beta-glucosidase activity and for the leucine-aminopeptidase activity. The assumption of homoscedasticity for the ANOVA was tested with the Levene's test which showed that both the data for the beta-glucosidase ($p = 0.07$) and the leucine-aminopeptidase ($p = 0.43$) was not in violation with this assumption. The one-way ANOVA established that there were no significant differences in the enzyme activity at different temperatures for the beta-glucosidase ($F(2,9) = 0.12$, $p = 0.89$) and the leucine aminopeptidase ($F(2,9) = 0.45$, $p = 0.65$).

Figure 13 Potential enzyme activities of (a) beta-glucosidase and (b) leucine-aminopeptidase for 2-, 5- and 9°C samples. Note: activity measurements were performed on 4 samples for each temperature. The measurement was performed at 6°C for all 12 samples.

3.2 Biological

3.2.1 DNA amounts as indicator of biomass

DNA amounts measured on the Qubit was used as an indicator of the quantity of microorganisms in the peat soil slurry to assess if there were changes in the microbial biomass from start to end of the experiment and between the temperature treatments (figure 14). In both the start and end samples the biomass variation was high. For the start samples, the DNA amount ranged from ~2700 ng/g soil in sample S09 to ~5700 ng/g in sample S01. In the end samples the highest measured amount was ~5300 ng/g soil in sample E09 and the lowest in sample E14 of ~2000 ng/g. The average amount was 4223 ng/g (95% CI = ± 364 ng/g) at the start and 3600 ng/g (95% CI = ± 397 ng/g) at the end. Overlapping CI signifies no statistically significant difference in the amount of DNA between the start and end samples.

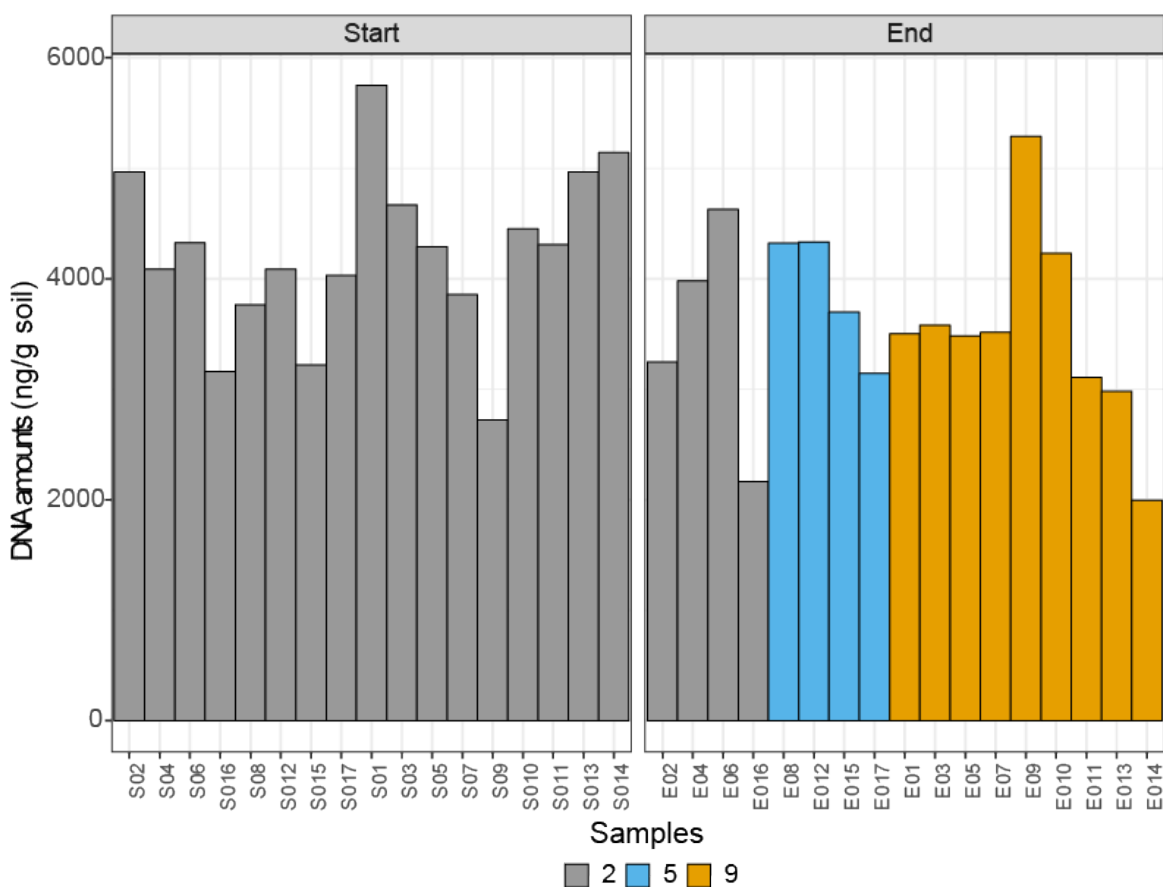


Figure 14 The amounts of DNA from extractions in ng of DNA per g of soil separated into start and end samples. Samples at 2°C marked in grey, samples of the 5°C treatment marked in blue, and samples of the 9°C treatment marked in orange.

The variation was also high within the temperature treatment groups of the end samples. The average DNA amount was 3505 ng/g soil (95% CI \pm 1036 ng/g) in the 2°C treatment end samples, 3874 ng/g soil (95% CI \pm 559 ng/g) in the 5°C treatment and 3520 ng/g soil (95% CI \pm 586 ng/g) in the 9°C treatment. The assumption of equal variances for the ANOVA was tested with a Levene's test, which showed that the data of the three groups of temperature treatment had similar variation ($p = 0.69$). An ANOVA analysis showed that there were no significant differences between the three groups of temperature treatment ($F(2,14) = 0.26$, $p = 0.78$), signifying equal amounts of DNA across all treatments.

3.2.2 Community composition

Analyses on the community composition was performed to identify differences in the community structure between the start and the end of the experiment. The 16S rRNA gene amplicon sequence libraries were composed on average by 0.8 % Archaea, 97.7% Bacteria and 1.5% which could not be assigned to a domain. Both start and end samples had highly similar abundances of Archaea and Bacteria, indicating no effect of temperature on the ratio of Bacteria to Archaea. The 20 most abundant OTUs belonged to Bacteria and belonged within the phyla Bacteroidetes, Actinobacteria, Verrucomicrobia, Proteobacteria, Firmicutes and Chloroflexi. The archaeal portion was composed of 61.3% Woesearchaeota, 21.9% belonging to unknown archaeal phyla, 13.8% Euryarchaeota, 1.56% Crenarchaeota, 0.32% Thaumarchaeota and 0.16% Altarchaeota.

3.2.2.1 Differences in community between start and end samples

A plot of the phyla representing more than 10% of the OTUs (figure 15) does not show any indication of differences in the abundance of phyla as a result of the temperature treatments. Furthermore, all the large phyla have similar abundances at the start and end.

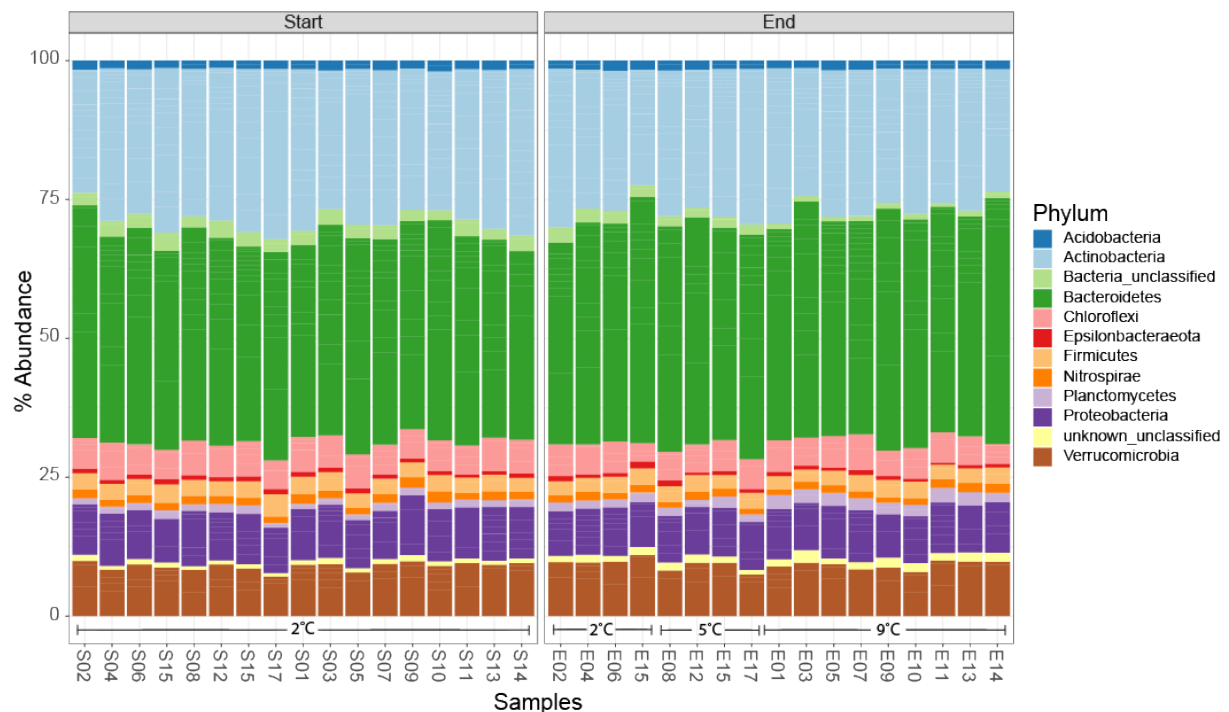


Figure 15 Distribution of abundances of the phyla representing >10% of the total data set. Faceted into start and end samples to visualise the relationship between time, temperature and the bacterial community composition.

The same type of plot only for archaeal phyla (figure 16) shows the same trend with similar distribution of the phyla at the start and end of the experiment. The two biggest phyla of Archaea were the Woesearchaeota and Euryarchaeota. A large portion of the archaeal sequences could not be assigned to an archaeal phylum and was thus named Archaea_unclassified.

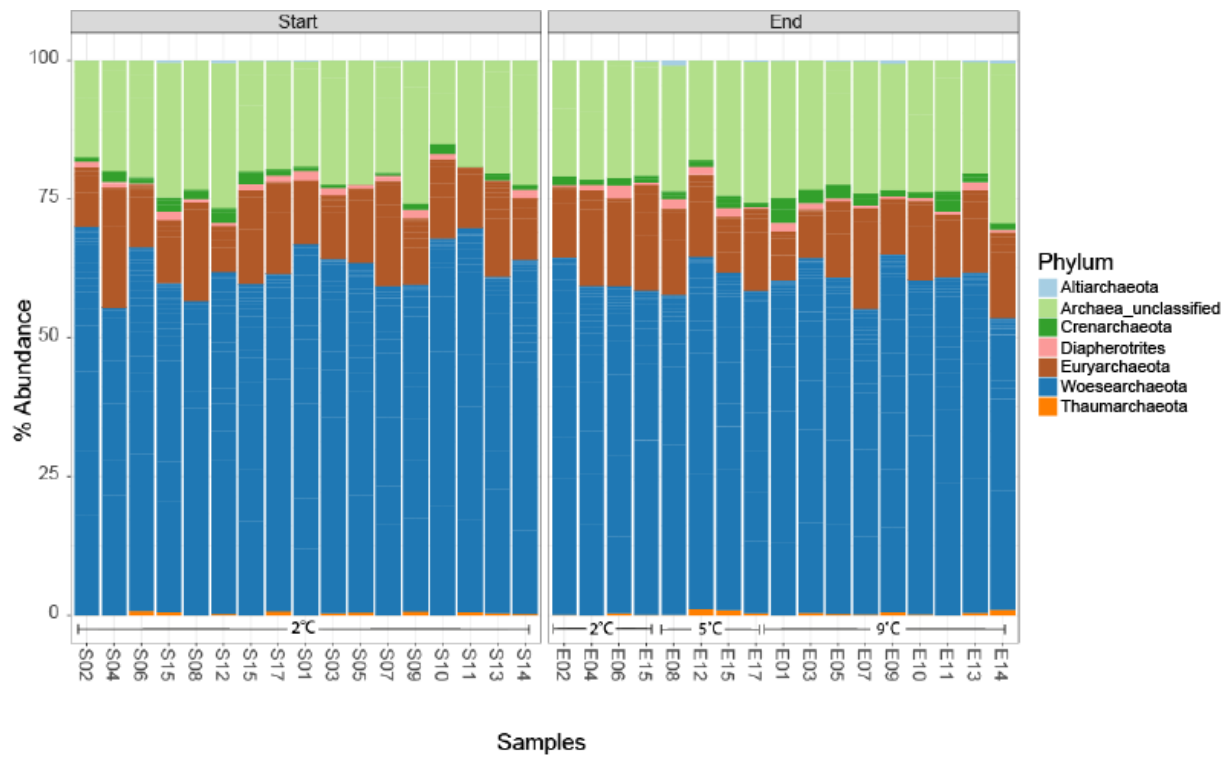


Figure 16 Distribution of abundances of all the phyla within the Archaea. Faceted into start and end samples to visualise the relationship between time, temperature and the archaeal community composition.

Euryarchaeota contain the methanogen classes Methanobacteria and Methanomicrobia as well as Thermoplasmata within which we find methylotrophic methanogens of the order Methanomasiliicoccales and non-methanogenic taxa within Thermoplasmatales (Poulsen, et al., 2013) (figure 17). The distribution of the classes was similar at the start and end of the experiment. However, there was a large variation in the abundances of these classes between samples, irrespective of the temperature treatments.

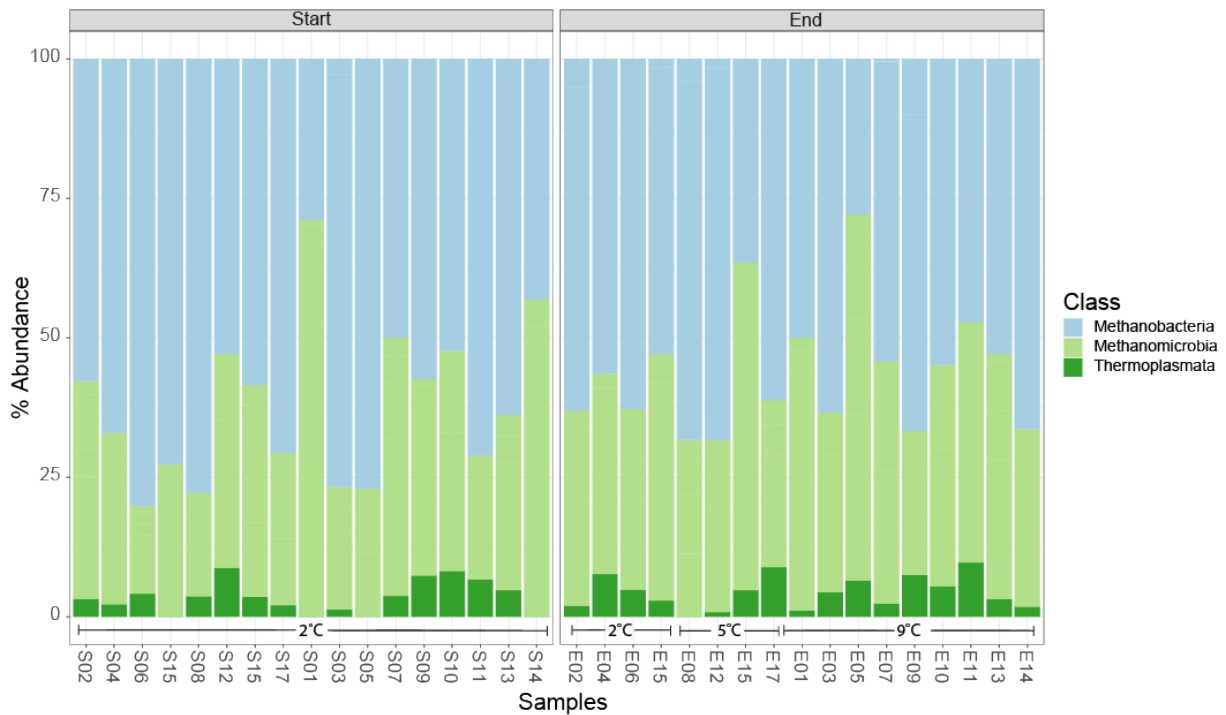


Figure 17 Abundance distribution of the classes represented within the Euryarchaeota phylum between start and finish and sorted for the temperature treatments, to visualise the relationship between time, temperature and the archaeal community composition.

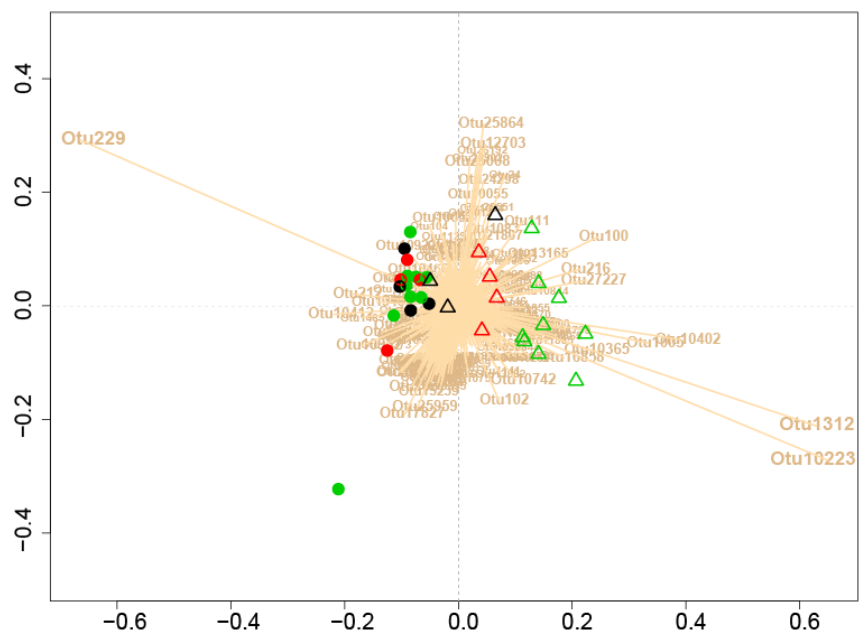
3.2.3 Correspondence analysis

The bacterial and archaeal communities were highly similar on the phylum and class level of taxonomy across time and temperature treatments. In order to test whether OTUs within these large taxonomic groups responded to the experimental treatments we decided to perform a correspondence analysis (CA) using the bacterial (figure 18.A) and archaeal OTU abundances (figure 18.B).

The Bacteria show a clear separation of start and end samples, as well as the different temperature treatments. The start samples are clustering at the negative side of the x-axis while the end samples are spreading out from the middle of the plot and toward the positive side of the x-axis. The 2°C control samples (black, open triangles figure 18.A) clustered close to the start samples, with the exception of one outlier sample, while the 5°C clustered between the start and 2°C on the left side of the plot and the 9°C samples which clustered furthest to the positive side of the x-axis. Three OTUs were very influential in separating the start and end samples. OTU 229 (unclassified Bacteria) pulled strongly in the neagtive direction of the x-axis, indicating that it has a higher abundance in the start samples and the samples at the lowest

temperature. OTU 1312 (unclassified Bacteria) and 10223 (VadinHA49, Planctomycetes) pulled strongly to the positive side of the x-axis suggesting that these OTUs have higher abundances in the end samples at the higher temperatures, 5 and 9°C. The samples showed weaker separation based on the Archaea community composition. We observed a clustering of start samples in the positive direction of the y-axis, and the end samples at the negative side of the y-axis. OTU 18328 (Bathyarchaea, Crenarchaeota) and 14226 (Woesearchaea, Woesearchaeota) pulled most downwards towards the negative y-axis indicating a higher abundance in the end and higher temperature samples, while OTU 10500 (Woesearchaea, Woesearchaeota) pulled strongly in the opposite direction indicating a higher abundance in the start and low temperature samples.

A Bacteria



B Archaea

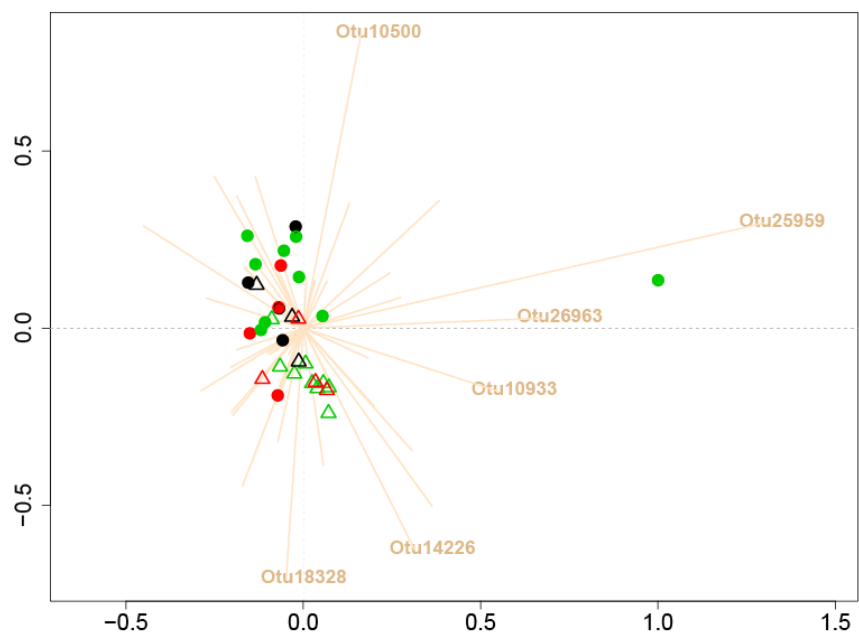
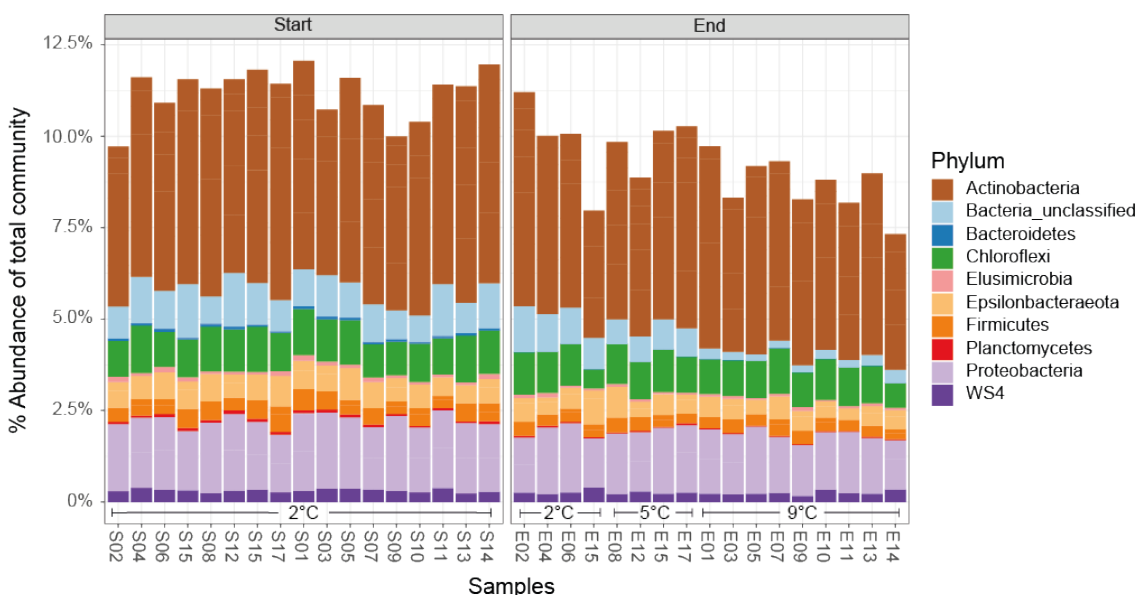


Figure 18 Correspondence analysis of (A) bacterial OTUs (99% threshold) and (B) archaeal OTUs (95% threshold). Start samples are marked as circle, end samples as open triangles. Green are the samples undergoing the 9°C treatment, red are the 5°C control samples and black are 2°C control samples. Sample E4 (2°C control sample) was removed from the CA.

3.2.4 Abundances of influential OTUs from CA

In addition to the 6 bacterial and archaeal OTUs indicated as the most temperature-responsive community members above we wanted to further broaden the search for temperature responsive OTUs. We selected the 20 most influential OTUs from both the negative and positive directions of the CA axes that separated the communities of Bacteria and Archaea by temperature and plotted them as bar plots (Figure 19).

A Most influential bacterial OTUs in the negative direction of the x-axis of the CA



B Most influential bacterial OTUs in the positive direction of the x-axis of the CA

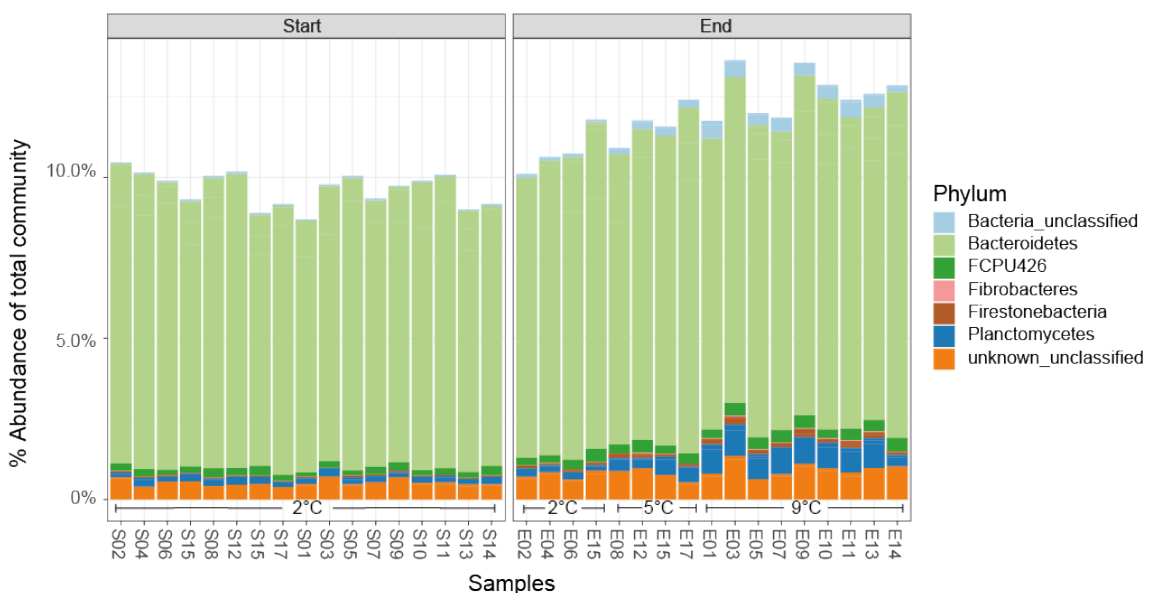
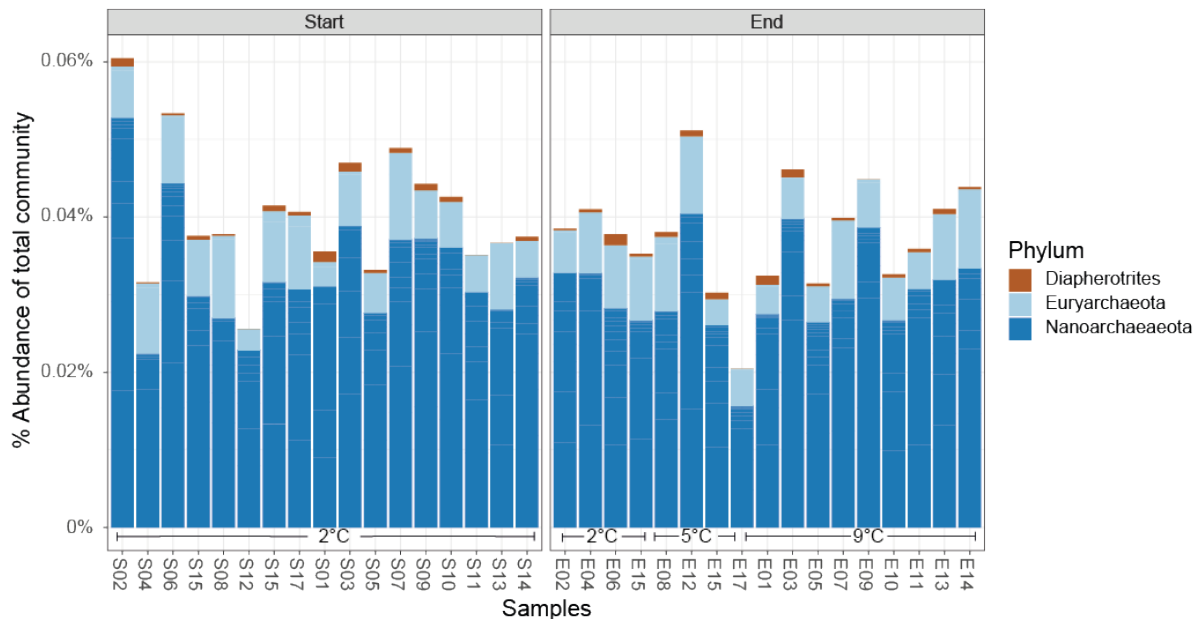


Figure 19 Abundance plot of the most influential OTUs of the Bacteria (A) pulling the start samples in the negative direction of the x-axis, and (B) pulling the end samples in the positive direction of the x-axis of the CA plot.

The abundance of the 20 most influential OTUs of the Bacteria pulling the start samples to the negative side of the x-axis shows a big proportion of Actinobacteria, Proteobacteria, and Chloroflexi (figure 19.A). The figure also shows that the differences in relative abundance of these OTUs between the low and high temperatures are small. The major exception to this was a decrease in the proportion of unclassified Bacteria in the end samples of the higher temperature incubations (5 and 9 °C). Altogether, the OTUs shown in figure 19.A made up 10 – 12% of the total community in the start samples and decreased to below 10% in the 9°C samples at the end of the incubation. It is also evident from the figure that more different OTUs respond to increased temperatures with a decrease in their relative abundance. The 20 most influential OTUs of the Bacteria of the CA plot that increased in abundance with increasing temperature (refer to figure 18.B) have very stable abundances within the start cluster. The largest proportion of these OTUs belong the Bacteroidetes phylum. The most prominent differences observed were higher abundances of the vadinHA49 (belonging to the Planctomycetes) class and some unclassified Bacteria at higher temperatures, while minor increases in OTUs belonging to Bacteroidetes and Firestonebacteria were also seen (figure 19.B).

For the start samples of the Archaea, three phyla where responsible for pulling the start samples in the positive direction of the y-axis. These were members of the Diapherotrites, Euryarchaeota and the Woesearchaeota (figure 20.A). The largest group was the Woesearchaeota which varied a lot between samples. The total abundance of these OTUs varied between 0.04 – 0.06% of the total community in the start samples, with no major differences in the end samples. The OTUs responsible for pulling the end samples in the negative direction of the y-axis were from a larger set of phyla (figure 20.B). The main constituents were the Woesearchaeota and some unclassified Archaea. The overall abundance was around 0.03% of the total community in the start samples but increase to between 0.04 – 0.05% in the higher temperatures of the end samples.

A Most influential archaeal OTUs in the positive direction of the y-axis of the CA



B Most influential archaeal OTUs in the negative direction of the y-axis of the CA

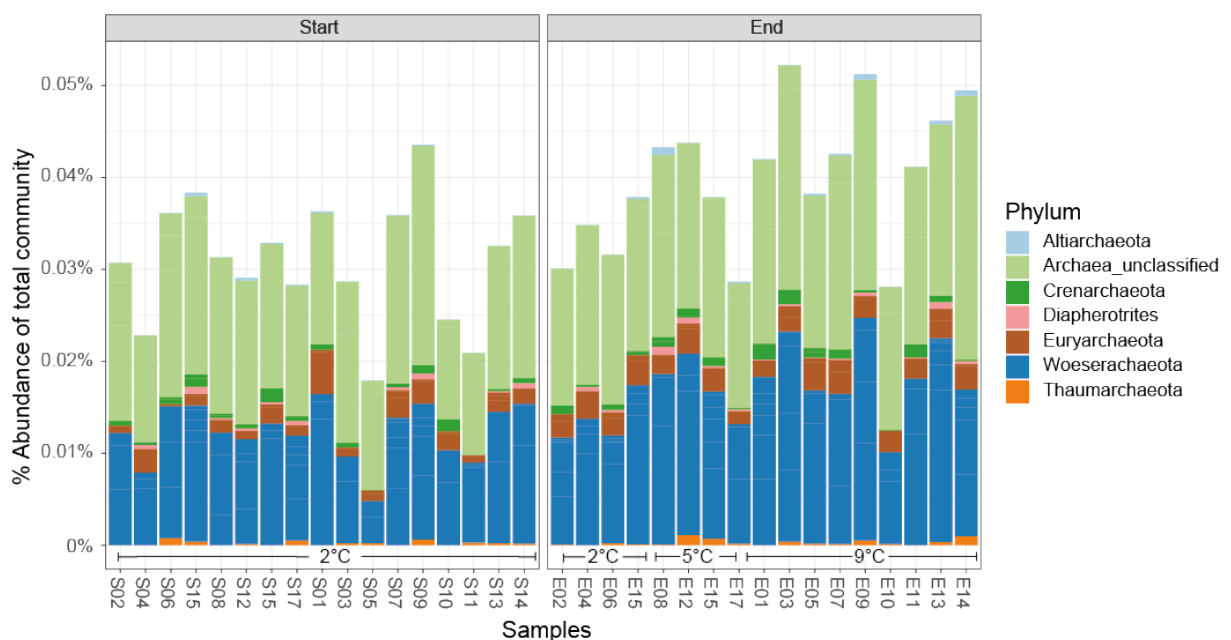


Figure 20 Abundance plot of the most influential OTUs of the Archaea (A) pulling the start samples towards the positive direction of the y-axis, and (B) pulling the end samples in the negative direction of the y-axis of the CA plots.

4 Discussion

4.1 Incubation temperatures

The initial incubation temperatures were supposed to be 2-, 4-, 6-, 8- and 10°C. However, due to a lack of incubator precision, 2-, 3-, 5-, 7.5- and 9°C were the average temperatures experienced by the microbial communities during incubation. These temperatures were still appropriate for investigating the effect of temperature increases as they occur at Svalbard in the transition from spring to summer. In the analyses, the average temperatures; 2-, 3-, 5-, 7.5- and 9°C; were used. However, it is important to recognize that the temperatures inside incubators varied on a daily basis. Especially, during days 27 to 49, the temperature of the 2°C incubator fluctuated substantially, (figure 6) but most of the variation was between 1.3°C and 2°C. This might have had an effect on the microbial productivity. In fact, a small reduction in the slope of the CH₄ production for the 2°C right around day 30 was observed (figure 8). It is therefore possible that the calculated CH₄ production rate for the 2°C incubations was slightly underestimated for the Arrhenius linear model. However, it is unlikely to have influenced our estimates or conclusions. Likewise, the actual temperature in what was supposed to be our 4°C incubation was lower and overlapping the temperature of the 2°C incubation for the same time period (figure 6). This probably explains why we did not observe changes in the CH₄ production rate after moving incubation flasks from 2°C to 3°C.

4.2 Primers

The primer pair chosen for the 16S amplicon sequencing (A519F and Bakt_805R) was chosen based on the high coverage reported for both Bacteria and Archaea (Klindworth, et al., 2013). Klindworth et al. (2013) highlights the bacterial and archaeal groups that the primers did not match, including the archaeal phylum Nanoarchaeaeota. Curiously, among the archaeal OTUs of our dataset as much as 61% was classified as Woesearchaeota, a close relative to the Nanoarchaeaeota that was not yet described in 2013. Furthermore, the abundance of Archaea was considerably smaller than what has been indicated previously from peat soil from the same area (Tveit, et al., 2015). Archaea only constitute ~1% of the dataset but was by Tveit et al. (2015) estimated to be 3 – 5% of the 16S rRNA genes and 6 – 9% of the rRNA. This indicates that a primer bias might have caused an underrepresentation of Archaea in the datasets.

However, in our opinion, as long as the main objective was to compare a set of samples to identify temperature driven changes in the community, the data still suffice. It could be argued that for a more realistic understanding of the communities and their composition, sequencing of the bacterial and archaeal communities separately using different, domain-specific, primer pairs could increase the accuracy of the taxonomic representation. The ratio of Bacteria to Archaea would not have been assessed precisely by this method, leaving PCR free shotgun-sequencing as a better but significantly more expensive method.

4.3 Gas production

The net CO₂ accumulation (figure 10) did not respond with a higher production rate with increasing temperature as observed for CH₄ (figure 8). In the first 10-15 days of the incubation the concentration of CO₂ was increasing sharply, most likely due to release of dissolved CO₂ in the liquid phase as the equilibrium of the CO₂ of the liquid and the headspace was unbalanced after flushing the headspace with N₂. The CO₂ production rates after this point were close to zero, but not entirely, meaning that there was an overall higher production than consumption. There was also a constant relationship between the temperature treatments showing that temperature had no effect on CO₂ accumulation. CO₂ production, like any enzyme catalyzed reaction, increases with temperature due thermokinetic effects on the enzymes as long as the CO₂ producing microorganisms do not redirect the carbon for growth instead of CO₂ production from energy generating processes (Bengtson & Bengtsson, 2007). However, the enzymes catalyzing the assimilation of CO₂ would also be affected by temperature increase. Thus, there are two possible reasons for our observations; either CO₂ is nearly not produced at all and there is no temperature effect on its production, or it is produced and then consumed, with both sides sharing the same temperature response. Both CH₄ and CO₂ are produced in energy generating processes where some of the carbon is assimilated for growth. CO₂ is consumed in many metabolic reactions such as CO₂ reduction with formylmethanofuran dehydrogenase by hydrogenotrophic methanogens, various carboxylase reactions and CO₂ fixation by autotrophs via a range of different pathways (Fuchs, 2011).

We observed a clear temperature effect on the production of CH₄. The rate of CH₄ production was equal for all samples during the entire incubation at 2°C and 3°C from day 0 up until day 22 when the sample flasks were moved to 5°C. The change in temperature from 2°C to 3°C did not seem to have an effect on the CH₄ production rates. This can simply be explained by the

variability in the incubator temperatures which in this case meant that the peat slurry flasks were at very similar temperatures (figure 6), differing by less than 0.5°C for most of the incubation time. When the samples were moved from 5°C to 7.5°C there was an immediate separation between the CH₄ production rate in those samples and the rate in the four samples that were left at 5°C according to the floating regression (figure 8). The rates inferred from the linear regression of the 5°C and 7.5°C however, does not correspond to the trend indicated in the floating regression, suggesting that small, possibly non-linear changes in the system state developing over time are not properly captured by linear regression.

Based on what we see from the floating regression, the biological adaptations, if any, to the new temperature must be fast. We did not observe any difference in the amount of polymer degrading enzymes produced between the 2-, 5—and 9°C incubations (figure 13.A and B). This means that there were no differences in the extracellular enzyme production by polymer degrading Bacteria. Furthermore, we found no substantial differences in the microbial communities between the temperature treatments that could directly explain the increases in CH₄ production. That raised the question if the increased CH₄ production rates from the community at higher temperatures were solely due to the effect of temperature on enzyme kinetics, something which has been indicated by Yvon-Durocher et al. (2014).

When looking at the data for the CH₄ production rates, it was clear in the case of the 5°C, 7.5°C and 9°C that the rates were biphasic. There were not enough 3°C time points to properly evaluate the biphasic nature of this temperature window, and the 2°C had already been at 2°C for around two years, meaning the system had already acclimatized to that temperature. The rates for the other temperatures were divided into ‘beginning’ and ‘acclimatized’. The results showed that the linear regression model with both ‘beginning’ and ‘acclimatized’ CH₄ production rates had a temperature dependence with an E_a of 1.05 which was in accordance with the E_a found by Yvon-Durocher et al. (2014) to apply for pure culture of methanogens, anaerobic community incubations and at the ecosystem level. However, a broad 95% CI, an R² of 0.65 and the rates of two of the temperatures falling below the 95% CI suggest that the model is suboptimal and that the rates right after temperature change therefore cannot be predicted by the Arrhenius equation. This is further supported by the improved fit of the regression after removing the ‘beginning’ points (figure 9.B) and the non-linear relationship between the rate and the temperature when only the rates for ‘beginning’ points were plotted (figure 9.C). These

analyses display how the temperature dependence of CH₄ production differs, depending on whether we take the acclimatization period into account or not, suggesting that the systems responsible for CH₄ production changes with time. As the rates of the ‘beginning’ periods are consistently lower than that of the ‘acclimatized’ at equivalent temperatures the system acclimatization during this time seems to be causing a delay in the production of CH₄. To our knowledge, very few have described this before.

The CH₄ produced by the anaerobic community is the product of methanogenesis from the combination of carbon substrates supplied through the breakdown of polysaccharides (Tveit, et al., 2015; Kotsyurbenko, 2005) and the decomposition of necromass from the microbial loop (Tveit, et al., 2015). As the temperature increases decomposition goes faster, which leads to an increase in the amount of carbon that goes into the production of CH₄ as well as growth (White, et al., 1991). The reason we see differences in the CH₄ production rates at different time points after temperature change could possibly be linked to shifts in the balance between carbon assimilation into biomass, death rates of the microbes and the production of CH₄. Essentially, the carbon processed in methanogenic decomposition might end up in different pools such as biomass or fermentation intermediates (Tveit, et al., 2015) before it reaches the end of the decomposition chain and is converted into CH₄. Thus, the predictive power of the Arrhenius equation on the temperature dependence of CH₄ production might not be the same if one considers the effect at different time points after the temperature change, something that was not considered in Yvon-Durocher et al. (2014).

4.4 Growth rates

At first glance the growth rates not only seemed to fit with the Arrhenius equation but also have the same temperature dependence as CH₄ production, with an E_a of 1.18 and overlapping 95% CI (figure 12.A). Yvon-Durocher et al.(2014) saw that the temperature dependence of the growth rate of a pure culture of methanogens was the same as for methanogenesis. However, our growth-data had two outliers at 2- and 5°C , which are dragging the linear regression to a steeper slope. When removing these outliers, it became obvious that a linear regression model was over all a bad fit, which means that the temperature dependence of the growth of the whole community cannot be inferred by the Arrhenius equation. What we see is that there were no significantly higher growth rates at 5°C compared to the growth rates at 2°C, but much higher

growth rates at 9°C (figure 11). The fact that the CH₄ production increases and the growth rate stays the same after increasing the temperature from 2 to 5°C indicates that the cells are mostly increasing their energy production, but not their investment into growth during this change. It is well known that organisms can live at temperatures beneath the range that allows growth and less energy is needed for survival and maintenance than for growth (Price & Sowers, 2004). However, growth was observed at both 2 and 5°C, just not an increase in growth from 2 to 5°C. Based on this, it is possible that at 5°C the temperature increases and the resulting increases in the fluxes of carbon, energy and nutrients are too low for the organisms to invest additional resources for growth within the timeframe of this experiment. Thus, an additional mechanism other than the growth and biomass conversion limitation hypothesized above might act as the bottleneck at 5°C.

4.5 Community composition

Despite the substantially higher growth rates at 9°C, there was not a corresponding increase in the amount of DNA present at the end compared to the start of the experiment (figure 14). This coincides with what has been shown previously (Tveit, et al., 2015), and can be seen in relation with a higher death rate due to predation by eukaryotic protists (Tveit, et al., 2015) and viral infections (Kuzyakow & Mason-Jones, 2018; Bratbak, et al., 1994). The resulting necromass can then be fed upon by necromass degraders who among other things degrade DNA, explaining why the biomass increase cannot be detected by DNA quantification methods (Morrissey, et al., 2015).

In trying to understand why the CH₄ production rates right after temperature change are lower than expected we propose that the energy and carbon going into the growth of the microbial biomass has not yet been balanced by death, which would cause imbalance between the carbon supplied for methanogenesis from polysaccharides and the necromass (figure 21). This could create a lag in the total CH₄ production as carbon from necromass is still supplied in rates similar to before temperature change. So, whereas there is an immediate response in the CH₄ production from the polysaccharides of plants, there is a phase where the supply of carbon from the necromass is the same as before temperature change, until death through predation, competition and/or virus infection catches up with the increased biomass. An increased death rate makes more necromass available for necromass degraders that can then move more carbon

into the CH₄ production, possibly through methylamines from degradation of amino acids and choline, which has been shown to be more important with increasing temperature (Tveit, et al., 2015).

As suggested above it is possible that parts of the lacking explanatory power of the Arrhenius equation (Yvon-Durocher et al. 2014) might derive from the temporal imbalance between increased biomass and death rates. We suggest that shortly after temperature change, enough carbon is still trapped in new microbial biomass that we cannot see the effect of temperature on the total CH₄ production. At first glance we did not observe changes in the community composition (figure 15-17), but the CA revealed that some of the most influential OTUs in differentiating the high temperature end samples from the start samples were members of the phylum Bacteroidetes (figure x). Microorganisms within Bacteroidetes has previously been indicated as taking part in the degradation of necromass (Müller, et al., 2018) and predation (Lueders, et al., 2006).

Members of the Planctomycetes also increased in relative abundance with increasing temperature. This fits with the observation of Planctomycetes as necromass degraders by Morrissey et al. (2015) who saw a correlation between the amount of extracellular DNA and the abundance of Planctomycetes. Tveit et al. (2015) showed in their study that the abundance of predatory protists increased with increasing temperature, displaying the most prominent shift in the entire microbial community. Having this in mind, the findings of increased abundances of putative necromass degraders with increasing temperature favors the notion that an increase in death rates and necromass decomposition is driven by temperature. While members of Bacteroidetes and Planctomycetes may have many different ecological roles in soil (Lueders, et al., 2006; Müller, et al., 2018; Morrissey, et al., 2015; Tveit, et al., 2013; Cobaugh, et al., 2015) we consider this as a plausible explanation for our findings that deserve further investigations.

In summary, it seems like part of the energy and carbon right after temperature change is still trapped in new organisms. As the biomass becomes balanced by predator- and virus-driven deaths, increased fluxes of necromass provide a window of opportunity in terms of energy, carbon and nutrients for increased growth rates of e.g. Planctomycetes and Bacteroidetes relative to other members of the microbial community. With the increased abundances of

necromass degraders as well as eukaryotic predators the system re-balances at a new steady state of growth-death balance after an initial biomass increase (figure 21).

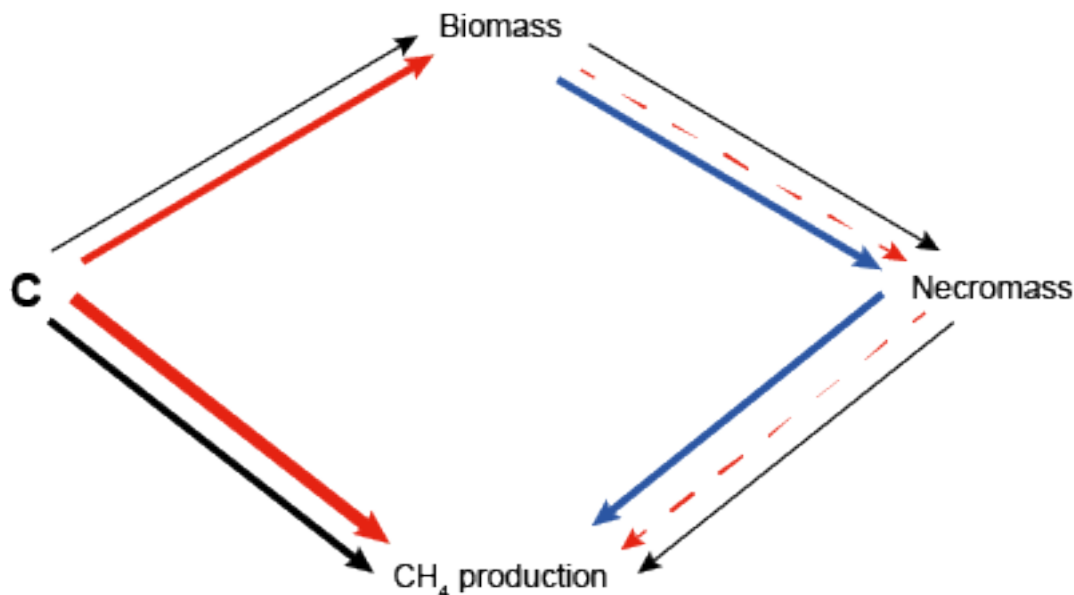


Figure 21 Proposed balance between carbon being used for biomass growth, CH_4 production and necromass degradation. Before temperature change (black arrows) carbon is sequestered into both biomass growth and CH_4 production. After the temperature increase more carbon is going into both the biomass and the CH_4 production (red, solid lines), but the number of deaths caused by predation and viral infection has not caught up, leading to the same amount of carbon going from the necromass into CH_4 production as before temperature change (red, dotted lines). When predators and viral infections catch up the death rates increase and as a response, necromass degraders starts feeding more carbon into the production of CH_4 (blue lines).

4.6 Temperature range

This study covers a narrower temperature range than most previous studies (Tveit, et al., 2015; Radujkovic, et al., 2018), and we see that the community of microorganisms which are present initially at 2°C can adapt to an increase in temperature up to 10°C with very few changes in its composition. With larger temperature increases the organisms of the initial community might not cope with the changes due to limited temperature ranges of enzyme function. Thus, more drastic shifts in the taxonomic composition may be observed at higher temperatures than in our narrow temperature range due to replacement of certain populations by taxa more suited for life at high temperatures.

5 Conclusion

Here we show that between 2 and 10°C, the temperature effect on CH₄ production can be explained by the Arrhenius equation if the system is granted sufficient time for acclimatization. Correspondingly, the CH₄ production rate during the initial stage after temperature change cannot be predicted by the Arrhenius equation, confirming that biological changes occur in the transition to the predictable rate. Thus, hypotheses 1 and 2 of section 1.5 are confirmed. This study thus highlights how time must be considered in order to predict temperature dependent changes in CH₄ production rates. Furthermore, we observed small shifts in the abundance of OTUs within Planctomycetes, Bacteroidetes and a few other taxa with increasing temperature, thus rejecting hypothesis 3. We suggest that these shifts are related to the observed temperature acclimatization that resulted in higher CH₄ production rates, hypothesizing that the responsive OTUs are involved in the degradation of accumulating necromass. The overall community did not change, indicating that the far majority are not disproportionately affected by temperature and systemic changes. Overall, we propose predation and viral infections or other death-causing mechanisms as the primary biological mechanisms that limit temperature effects on CH₄ production.

6 Outlook

To confirm the proposed mechanisms behind the low CH₄ production of the initial stage after temperature change, quantification of DNA and RNA after and before temperature change could be done to confirm changes in biomass in the acclimatization stage, and metagenomics and transcriptomics to look at predatory protist and function of putative necromass degraders. Isotope labelling of necromass and SIP-metagenomics could also be performed to look at the incorporation of the label in necromass degraders to track their identity. Furthermore, shotgun-sequencing could be used to avoid primer biases, as we saw some indications that the A519F and Bakt_805R produced some biases.

References

- Anisimov, O. D. V. T. C. C. F. H. M. T. P. H. V. a. J. W., 2007. Polar regions (Arctic and Antarctic). Climate Change 2007: Impacts, Adaptation and Vulnerability. Contribution of Working Group II to the Fourth Assessment Report of the Intergovernmental Panel on Climate Change.. *Cambridge University Press*, Volume AR5, pp. 653-658..
- Bekryaev, R., Polyakov, I. & Alexeev, V., 2010. Role of Polar Amplification in Long-Term Surface Air Temperature Variations and Modern Arctic Warming. *Journal of Climate*, 23(14), pp. 3888-3906.
- Bengtson, P. & Bengtsson, G., 2007. Rapid turnover of DOC in temperate forests accounts for increased CO₂ production at elevated temperatures. *Ecology Letters*, 10(9), pp. 783-790.
- Blaha, D. et al., 1999. Natural and anthropogenic methane sources in New England. *Atmospheric Environment*, 33(2), pp. 243-255.
- Bousquet, P. et al., 2006. Contribution of anthropogenic and natural sources to atmospheric methane variability. *Nature*, Volume 443, pp. 439-443.
- Boylen, E. & al., e., 2018. QIIME2: Reproducible, interactive, scalable, and extensible microbiome data science. *PeerJ preprints*, p. 6:e27295v2.
- Bradley, J., Amend, J. & LaRowe, D., 2018. Necromass as a Limited Source of Energy for Microorganisms in Marine Sediments. *Journal of Geophysical Research: Biogeosciences*, Volume 2.
- Bratbak, G., Thingstad, F. & Heldal, M., 1994. Viruses and the Microbial Loop. *Microbial Ecology*, pp. 209-211.
- Breeuwer, A. et al., 2009. Decreased summer water table depth affects peatlands vegetation. *Basic and Applied Ecology*, 10(4), pp. 330-339.
- Buan, N. R., 2018. Methanogens: pushing the boundaries of biology. *Emerging Topics in Life Sciences*, 2(4), pp. 629-646.
- Bugg, T., Ahmad, M., Hardiman, E. & Rahmanour, R., 2011. Pathways for degradation of lignin in bacteria and fungi. *Natural Product Reports*, Volume 28, pp. 1883-1896.
- Cobaugh, K., Schaeffer, S. & DeBruyn, J., 2015. Functional and Structural Succession of Soil Microbial Communities below Decomposing Human Cadavers. *PLoS One*, 10(6), p. e0130201.

Conrad, R., 1999. Contribution of hydrogen to methane production and control of hydrogen concentrations in methanogenic soils and sediments. *FEMS Microbiology Ecology*, 28(3), pp. 193-202.

Edgar, R., 2010. Search and clustering order of magnitude faster than BLAST. *Bioinformatics*, 26(19), pp. 246-2461.

Enzmann, F., Mayer, F., Rother, M. & Holtmann, D., 2018. Methanogens: biochemical background and biotechnological applications. *AMB Express*, 8(1).

Etiope, G. & Lollar, B., 2013. Abiotic Methane on Earth. *Reviews of Geophysics*, 51(2), pp. 276-299.

Feller, G. & Gerday, C., 2003. Psychrophilic enzymes: hot topics in cold adaption. *Nature Reviews Microbiology*, Volume 1, pp. 200-208.

Fenner, N. & Freeman, C., 2011. Drought-induced carbon loss in peatlands. *Nature Geoscience*, Volume 4, pp. 895-900.

Fernandez, A. et al., 1999. How Stable is Stable? Function versus Community Composition. *Appl Environ Microbiol*, 65(8), pp. 3697-3704.

Ferry, J., 2010. Biochemistry of acetotrophic methanogenesis. *Handbook of Hydrocarbon and Lipid Microbiology*, pp. 357-367.

Freeman, C., Ostle, N. & Kang, H., 2001. An enzymatic 'latch' on the global carbon store. *Nature*, Volume 409, p. 149.

Freeman, W. & Macmillan, P., 2013. Chapter 7: Photosynthesis, Light and Life. In: *Raven Biology of Plants*. New York: W.H. Freeman and Company, pp. 129-139.

Friedman, S., Axel, R. & Weisntein, I., 1967. Stability of Ribosomes and Ribosomal Ribonucleic Acid from *Bacillus stearothermophilus*. *Journal of Bacteriology*, 93(5), pp. 1521-1526.

Frolking, S. et al., 2011. Peatlands in the Earth's 21st century climate system. *Environmental Reviews*, Volume 19, pp. 371-396.

Fuchs, G., 2011. Alternative Pathways of Carbon Dioxide Fixation: Insight into the Early Evolution of Life. *Annual Reviews Microbiology*, Volume 65, pp. 631-658.

Gonzales, T. & Robert-Baudouy, J., 1996. Bacterial aminopeptidases: Properties and functions. *FEMS Microbiology Reviews*, 18(4), pp. 319-344.

- Grosjean, H. & Oshima, T., 2007. How Nucleic Acids Cope with High Temperatures. *Physiology and Biochemistry of Extremophiles.*, pp. 39-56.
- Hoehler, T. & Alperin, M., 2014. Methane minimalism. *Nature*, Volume 507, pp. 436-437.
- Holland, M. & Bitz, C., 2003. Polar amplification of climate change in coupled models. *Climate Dynamics*, 21(3-4), pp. 221-232.
- Hultman, J. et al., 2015. Multi-omics of permafrost, active layer and thermokarst bog soil microbiomes. *Nature*, 521(7551), pp. 208-212.
- Janusz, G. et al., 2017. Lignin degradation: microorganisms, enzymes involved, genomes analysis and evolution. *FEMS Microbiol Rev*, 41(6), pp. 941-962.
- Joosten, H. & Couwenberg, J., 2008. Peatlands and carbon. *Assessment on peatlands, biodiversity and climate change*, pp. 99-117.
- Kalenitchenko, D., 2018. CAGE_MiSeq_SOP.sh. *GitHub Repository*.
- Karni, M. et al., 2013. Thermal Degradation of DNA. *DNA and Cell Biology*, 32(6), pp. 1-4.
- Keegstra, K., 2010. Plant Cell Walls. *Plant Physiol.*, 154(2), pp. 483-486.
- Klindworth, A. et al., 2013. Evaluation of general 16S ribosomal RNA gene PCR primers for classical and next-generation sequencing-based diversity studies. *Nucleic Acids Research*, 41(1), p. e1.
- Kotsyurbenko, O., 2005. Trophic interactions in the methanogenic microbial community of low-temperature terrestrial ecosystems. *FEMS Microbiology Ecology*, 53(1), pp. 3-13.
- Kumar, S., Stecher, G., Knyaz, C. & Tumara, K., 2018. MEGA X: Molecular Evolutionary Genetics Analysis across computing platforms. *Molecular Biology and Evolution*, Volume 35, pp. 1547-1549.
- Kuzyakow, Y. & Mason-Jones, K., 2018. Viruses in soil: Nano-scale undead drivers of microbial life, biogeochemical turnover and ecosystem functions. *Soil Biology and Biochemistry*, Volume 127, pp. 305-317.
- Los, D., 2004. The effect of low-temperature-induced DNA supercoiling on the expression of the desaturase genes in *Synechocystis*. *Cell Molecular Biology*, 50(5), pp. 605-612.
- Los, D., Horvath, I., Vigh, L. & Murata, N., 1993. The temperature-dependent expression of the desaturase gene desA in *Synechocystis* PCC6803. *FEBS Letters*, 318(1), pp. 57-60.

Louca, S. et al., 2016. High taxonomic variability despite stable functional structure across microbial communities. *Nature Ecology & Evolution*, 1(0015).

Lueders, T. et al., 2006. Identification of Bacterial Micropredators Distinctively Active in a Soil Microbial Food Web. *Applied and Environmental Microbiology*, 72(8), pp. 5342-5348.

Lynd, L., Weimer, P., van Zyl, W. & Pretorius, I., 2002. Microbial Cellulose Utilization: Fundamentals and Biotechnology. *Microbiology and Molecular Biology Reviews*, 66(3), pp. 506-577.

Madigan, M. et al., 2015. *Brock Biology of Microorganisms*. 14th ed. ed. Harlow: Pearson Education Limited.

Marr, A. & Ingraham, J., 1962. Effect of temperature on the composition of fatty acids in Escherichia coli.. *Journal of Bacteriology*, 84(6), pp. 1260-1267.

Mauro, V. & Matsuda, D., 2016. Translation regulation by ribosomes: Increased complexity and expanded scope. *RNA Biology*, 13(9), pp. 748-755.

Mayer, F. et al., 2015. Na⁺ Transport by the A1A0-ATP Synthase Purified from Thermococcus onnurineus and Reconstituted into Liposomes. *The journal of biological chemistry*, 290(11), pp. 6994-7002.

McLatchey, G. & Reddy, K., 1998. Regulation of Organic Matter Decomposition and Nutrient Release in a Wetland Soil. *Journal of Environmental Quality*, 27(5), pp. 1268-1274.

McLatchey, G. & Reddy, K., 1998. Regulation of organic matter decomposition and nutrient release in a wetland soil. *Journal of Environmental Quality*, 27(5), pp. 1268 - 1274.

McMillan, D. et al., 2011. A1AO-ATP synthase of MEthanobrevibacter ruminantium Couples Sodium Ions for ATP synthesis under Physiological Conditions. *The Journal of Biological Chemistry*, 286(46), pp. 39882-29892.

McMurdie, P. & Holmes, S., 2013. Phyloseq, An R Package for Reproducible Interactive Analysis and Graphics of Microbiome Census Data. *PloS ONE*, Volume 4, p. e61217.

Morrissey, E. et al., 2015. Dynamics of extracellular DNA decomposition and bacterial community composition in soil. *Soil Biology and Biochemistry*, Volume 86, pp. 42-49.

Mucha, H., Lingens, F. & Trösch, W., 1988. Conversion of propionate to acetate and methane by syntrophic consortia. *Appl Microbiol Biotechnol*, Volume 27, pp. 581-586.

Murrell, J., 2010. The aerobic methane oxidizing bacteria (methanotrophs). *Handbook of hydrocarbon and lipid microbiology*, pp. 1953-1966.

Myhre, G. S. D. et al., 2013. Anthropogenic and Natural Radiative Forcing. Climate change 2013: The Physical Science Basis. Working Group I Contribution to the Fifth Assessment Report of the Intergovernmental Panel on Climate Change. *Cambridge University Press*, Volume AR5, p. 1583 pp.

Müller, A. et al., 2018. Bacterial interactions during sequential degradation of cyanobacterial necromass in a sulfidic arctic marine sediment. *Environmental Microbiology*, 20(8), pp. 2927-2940.

Noble, A. et al., 2019. Peatland vegetation change and establishment of re-introduced Sphagnum moss after prescribed burning. *Biodiversity and Conservation*, 28(4), pp. 939-952.

Oliverio, A., Bradford, M. & Fierer, N., 2016. Identifying the microbial taxa that consistently respond to soil warming across time and space. *Global Change Biology*, 23(5), pp. 2117-2129.

Oswald, K. et al., 2017. Crenothrix are major methane consumers in stratified lakes. *The ISME Journal*, pp. 2124-2140.

Page, S., Rieley, J. & Banks, C., 2011. Global and regional importance of the tropical peatland carbon pool. *Global Change Biology*, 17(2).

Pancost, R. D. J., de Lint, S., dan der Maarel, M. & Gottschal, J., 2000. Biomarker Evidence for Widespread Anaerobic Methane Oxidation in Mediterranean Sediments by a Consortium of Methanogenic Archaea and Bacteri. *Applied and Environmental Microbiology*, 66(3), pp. 1126-1132.

Permafrost Subcommittee, 1988. Glossary of permafrost and related ground-ice terms. *Associate Committee on Geotechnical Research, National Research Council of Canada*.

Petsko, G. & Ringe, D., 2009. Proteins are linear polymers of amino acids connected by amide bonds. In: *Protein Structure and Function*. Oxford: Oxford University Press, p. 8.

Poulsen, M. et al., 2013. Methylotrophic methanogenic Thermoplasmata implicated in reduced methane emissions from bovine rumen. *Nature Communications*, Volume 4, p. 1428.

Price, P. & Sowers, T., 2004. Temperature dependence of metabolic rates for microbial growth, maintenance, and survival. *Proceedings of the National Academy of Sciences*, 101(13), pp. 4631-4636.

Pucciarelli, S. et al., 2005. Ribosomal cold-adaption: Characterization of the genes encoding the acidic ribosomal P0 and p2 proteins from the Antarctic ciliate Euplotes focialis. *Gene*, 360(2), pp. 103-110.

R Core Team, 2018. R: A language and environment for statistical computing..

Radestock, S. & Gohlke, H., 2011. Protein rigidity and thermophilic adaption. *Proteins: Structure, Function, and Bioinformatics*, 79(4), pp. 1089-1108.

Radujkovic, D. et al., 2018. Prolonged exposure does not increase soil microbial community compositional response to warming along geothermal gradients. *FEMS Microbiology Ecology*, 94(2).

Ramsay, I. & Pullammanappallil, P., 2001. Protein degradation during anaerobic wastewater treatment, derivation of stoichiometry. *Biodegradation*, Volume 12, pp. 247-257.

Ratkowsky, D. et al., 1983. Model for Bacterial Culture Growth Rate Throughout the Entire Biokinetic Temperature Range. *Journal of Bacteriology*, 154(3), pp. 1222-1226.

Reeburgh, W., 2007. Oceanic Methane Biogeochemistry. *Chemical Review*, Volume 107, pp. 486-513.

Reuveni, S., Ehrenberg, M. & Paulsson, J., 2017. Ribosomes are optimized for autocatalytic production. *Nature*, Volume 547, pp. 293-297.

Rognes, T. et al., 2018. VSEARCH, a versatile open source tool for metagenomics. *PeerJ*, Volume 4, p. e2584.

Samir, P. et al., 2018. Identification of changing ribosome protein composition using Cryo-EM and mass spectrometry. *Proteomics*, 18(20).

Sarkar, P., Bosneaga, E. & Auer, M., 2009. Plant cell walls throughout evolution: towards a molecular understanding of their design principles. *Journal of Experimental Botany*, 60(13), pp. 3615-3635.

Schloss, P. et al., 2009. Introducing mothur: Open-source, Platform-independent, Community-supported Software for Describing and Comparing Microbial Communities. *Applied and Environmental Microbiology*, 75(23), pp. 7537-7541.

Schoell, M., 1988. Multiple origins of methane in the Earth. *Chemical Geology*, 71(1-3), pp. 1-10.

Schouten, S. et al., 2003. Biogeochemical Evidence that Thermophilic Archaea Mediate the Anaerobic Oxidation of Methane. *Applied and Environmental Microbiology*, 69(3), pp. 1680-1686.

Schouten, S., Wakeham, S. & J.S.S., D., 2001. Evidence for anaerobic methane oxidation by archaea in euxinic waters of the Black Sea. *Organic Geochemistry*, 32(10), pp. 1277-1281.

Scott, M., Klumpp, S., Mateeschu, E. & Hwa, T., 2014. Emergence of robust growth laws from optimal regulation of ribosome synthesis. *Molecular Systems Biology*, Volume 10, p. 747.

Siddiqui, K. et al., 2006. Role of lysine versus arginine in enzyme cold adaptation: Modifying lysine to homo-arginine stabilizes the cold adapted α -amylase from Pseudoalteromonas haloplanktis. *Proteins: Structure, Function and Bioinformatics*, 64(2), pp. 480-501.

Solomon, S. et al., 2007. Technical summary. In: Climate change 2007: The Physical Science Basis. Contribution of Working Group I to the Fourth Assessment Report of the Intergovernmental Panel on Climate Change.

Strack, M. et al., 2008. Northern Peatlands, greenhouse gas exchange and climate change. *Peatlands and climate change*, pp. 44-69.

Sun, J., Tian, C., Diamond, S. & Glass, N., 2012. Deciphering Transcriptional Regulatory Mechanisms Associated with Hemicellulose Degradation in Neurospora crassa. *Eukaryotic Cell*, 11(4), pp. 482-493.

Tamura, K. & Nei, M., 1993. Estimation of the number of nucleotide substitutions in the control region of mitochondrial DNA in humans and chimpanzees. *Molecular Biology and Evolution*, Volume 10, pp. 512-526.

Tarnocai, C. et al., 2009. Soil organic carbon pools in the northern circumpolar permafrost region. *Global Biogeochemical Cycles*, 23(2).

Tarnocai, C. et al., 2009. Soil organic carbon pools in the northern circumpolar permafrost region. *Global biogeochemical Cycles*, 23(2).

Taylor, A., 1993. Aminopeptidases: structure and function.. *The FASEB journal*, 7(2), pp. 290-298.

Terui, Y. et al., 2005. Stabilization of nucleic acids by unusual polyamines produced by an extreme thermophile, Thermus thermophilus. *Biochemical Journal*, 388(2), pp. 427-433.

Thauer, R., 2012. The Wolfe cycle comes full circle. *PNAS*, 109(38), pp. 15084-15085.

Thauer, R. et al., 2008. Methanogenic archaea: ecologically relevant differences in energy conservation. *Nature Reviews Microbiology*, Volume 6, pp. 579-591.

The Human Microbiome Project Consortium, 2012. Structure, function and diversity of the healthy human microbiome. *Nature*, Volume 486, pp. 207-214.

- Thornton, P., 2010. Livestock production: recent trends, future prospects. *Philos Trans R Soc Lond B Biol Sci*, 365(1554), pp. 2853-2867.
- Timmers, P. et al., 2017. Reverse Methanogenesis and Respiration in Methanotrophic Archaea. *Archaea*.
- Tveit, A., 2014. *Microbial communities and metabolic networks in Arctic peatlands*, Tromsø: UiT The Arctic University of Norway.
- Tveit, A., In Prep. Temporal dynamics of peat decomposition shows that presumed identical system, originating from the same sample, develop different overall production rates over time.
- Tveit, A., Schwacke, R., Svenning, M. & Urich, T., 2013. Organic carbon transformations in high-Arctic peat soils: key functions and microorganisms. *The ISME journal*, 7(2), pp. 299-311.
- Tveit, A., Urich, T., Frenzel, P. & Svenning, M., 2015. Metabolic and trophic interactions modulate methane production by Arctic peat microbiota in response to warming. *PNAS*, 112(19), pp. 2507-2516.
- Valentine, R. & Wolfe, R., 1963. Role of ferredoxin in the metabolism of molecular hydrogen. *Journal of Bacteriology*, 85(5), pp. 1114-1120.
- Van Acker, R. et al., 2013. Lignin biosynthesis perturbations affect secondary cell wall composition and saccharification yield in *Arabidopsis thaliana*. *Biotechnology for Biofuels*, 6(1), p. 46.
- Vanwonterghem, I. et al., 2014. Deterministic processes guide long-term synchroinsed population dynamics in replicate anaerobic digesters. *ISME J*, 8(10), pp. 2015-2028.
- Walker, T. et al., 2018. Microbial temperature sensitivity and biomass change explain soil carbon loss with warming. *Nature Climate Change*, Volume 8, pp. 885-889.
- White, P., Kalff, J., Rasmussen, J. & Gasol, J., 1991. The Effect of Temperature and Algal Biomass on Bacterial Production and Specific Growth Rate in Freshwater and Marine Habitats. *Microbial Ecology*, Volume 21, pp. 99-118.
- Whitman, W., Bowen, T. & Boone, D., 2006. Chapter 9: The Methanogenic Bacteria. *Prokaryotes*, Volume 3, pp. 165-207.
- Wickham, H., 2016. ggplot2: Elegant Graphics for Data Analysis. *Springer-verlag*.

- Xu, J., Morris, P., Liu, J. & Holden, J., 2018. PEATMAP: Refining estimates of global peatland distribution based on meta-analysis. *Catena*, Volume 160, pp. 134-140.
- Yu, Z., 2012. Northern peatland carbon stocks and dynamics: a review. *Biogeosciences*, 9(10), pp. 4071-4085.
- Yu, Z. et al., 2010. Global peatland dynamics since the Last Glacial Maximum. *Geophysical Research Letters*, 37(13).
- Yvon-Durocher, G. et al., 2014. Methane fluxes show consistent temperature dependence across microbial to ecosystem scales. *Nature*, Volume 507, pp. 488-491.
- Zabranska, J. & Pokorna, D., 2018. Bioconversion of carbon dioxide to methane using hydrogen and hydrogenotrophic methanogens. *Biotechnology advances*, 36(3), pp. 707-720.
- Zydowsky, L. et al., 1987. Stereochemical Course of Methyl Transfer from Methanol to Methyl Coenzyme M in Cell-Free Extracts of *Methanosarcina barkeri*. *Journal of the American Chemical Society*, 109(25), pp. 7922-7923.

Appendix I: Materials and methods

A Determination of microbial growth: DNA extraction protocol.

Quantification of dsDNA with PicoGreen

(Quant-iT™ PicoGreen, life technologies Ref P11496)

Table 1. Contents and Storage Information.

Material	Amount	Concentration	Storage	Stability
A Quant-iT™ PicoGreen® dsDNA reagent (Component A)	1 mL in 1 vial (P7589) or in 10 vials of 100 µL each (P11496)	Solution in DMSO	+ 2–6°C • Desiccate • Protect from light	When stored as directed, product stable for at least 6 months
B 20X TE (Component B)	25 mL	200 mM Tris-HCl, 20 mM EDTA, pH 7.5	+ Room temperature *	
C Lambda DNA standard (Component C)	1 mL	100 µg/mL in TE	+ 2–6°C *	

* For long-term storage, both the 20X TE and lambda DNA standard can be stored at ≤-20°C.

Number of Labelings: For either the kits or the stand-alone reagent, sufficient reagent is supplied for 200 assays using an assay volume of 2 mL and the protocol described below. Note that the assay volume is dependent on the instrument used to measure fluorescence; with a microplate reader and a 96-well microplate, the assay volume is reduced to 200 µL and 2,000 assays are possible.

Spectral Data: Quant-iT™ PicoGreen® dsDNA reagent 502/523 nm, bound to nucleic acids

A) stored locked in "safe" in fridge / main lab

B) long-term storage at -20°C; aliquot in use can be kept at -4 °C for several weeks

C) long-term storage at -20°C; avoid freezing/thawing!! (once having thawed, prepare "reasonable" aliquots (e.g.: freeze 6 µL DNA standard, 100 µg/mL in TE, in a 1.5 mL eppi), that have to be thawed only once when being used)

-) dilute the 20X TE (Tris-EDTA) buffer to get a 1X TE buffer (1:20)

Dilute the 20X TE buffer 1:20 with sterile, distilled, DNase-free water (alternatively to DNase-free water, autoclaved MQ-water, 120 °C for 60 min, can be used).

Total amount of 1X TE buffer needed for a set of 50 samples + 2 std. rows (= 2 x 7 stds.) + 4 blanks (2 blanks per each std. row):

- 1X TE needed for sample dilution (e.g. 1:300)

$$3 \mu\text{L DNA extract} + 897 \mu\text{L 1X TE} \rightarrow 50 \times 897 \mu\text{L} = \underline{\underline{44.85 \text{ mL 1X TE}}}$$

- 1X TE needed for PicoGreen preparation (i.e. 1:200 dilution of PicoGreen to get PicoGreen-working solution, PG-WS)

Total amount of samples (incl. std.s and blanks): $50 + 14 + 4 = 68$

$$68 \times 100 \mu\text{L PG-WS} = 6.8 \text{ mL PG-WS is needed}$$

So for preparation of, for example, 8 mL Picogreen: $40 \mu\text{L Picogreen} + \underline{\underline{7.96 \text{ mL 1X TE}}}$

- 1X TE needed for all DNA stds. and blanks:

$$\underline{\underline{1.533 \text{ mL 1X TE}}}$$

- 1X TE needed for DNA working solution (DNA-WS) for 14 stds.:

0.294 ml. 1X TE

In total you need: $44.85 + 7.96 + 1.533 + 0.294 = 54.639 \text{ mL } 1\text{X TE}$

So prepare e.g. 50 mL 1X TE

-) dilute the DNA extracts with 1X TE in eppis

After having diluted the DNA extracts pipette each 100 µL in a black microtiter plate

-> prepare DNA-WS

Dilute the DNA-stock [100 µg/mL INTE] 1:50 with 1X TE to get a DNA-WS of 2 µg/mL. For a total of 14 stds. you need 267.5 µL DNA-WS; so prepare 300 µL of DNA-WS.

6 μ L DNA-SS + 294 μ L 1X TE

Pipette your DNA stds. and blanks in the black microtiter plate

-) Pipetting scheme:

		1	2	3	4	5	6	7	8	9	10	11	12
A	µL DNA-W5	50	37.5	25	12.5	5	2.5	1.25	0	0			
	µL 1XTE	50	62.5	75	87.5	95	97.5	98.75	100	100			
B													
C	nat. Ab.												
D													
E													
F	1AO												
G													
H	µL DNA-W5	50	37.5	25	12.5	5	2.5	1.25	0	0			
	µL 1XTE	50	62.5	75	87.5	95	97.5	98.75	100	100			

-) dilute the PicoGreen reagent 200fold (1:200) with 1X TE

Prepare this reagent in a plastic vial (e.g. 5 mL Eppi, 15 mL Greiner etc.), as the reagent may adsorb to glass surfaces. Protect the PG-WS from light by covering it with aluminum foil or placing it in the dark to avoid photodegradation. For best results, this solution should be used within a few hours of its preparation.

When handling with PicoGreen always work in the fume hood!

Wear protective gloves against toxic stuff! (Kimtech science purple nitrile xtra gloves 97610)

-) sample analysis

- Add each 100 µL of PG-WS to samples/stds and blanks. (use a multipipette)
- Incubate plate at room temperature in the dark for 5 minutes
- Measure fluorescence:

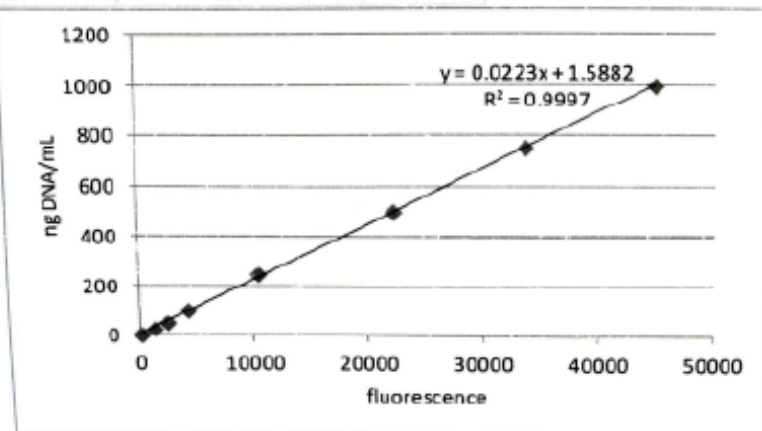
Excitation: 480 nm

Emission: 520 nm

Gain: optimal (each plate must have a standard row!)

Shaking: 10 seconds / 1mm orbital amplitude

	fluo	ng DNA	ng/mL
std1	44813	100	1000
std2	33623	75	750
std3	22256	50	500
std4	10415	25	250
std5	4195	10	100
std6	2371	5	50
std7	1263	2.5	25
bl1	111	0	0
bl2	82	0	0



B Determination of microbial growth: DNA quantification with PicoGreen (Quanti-iT™ PicoGreen, Life Technologies).

DNA Extraction Protocol for CUE (MP BIO DNA FAST SPIN KIT)

Centrifugations: use Beckmann Avanti™ 30 centrifuge in the soil lab. Rotor: F2402H

- 1) Add 100 ml 98% ethanol (Added Ethanol should be as pure as possible. Do not use Ethanol < 96%) to the concentrated SEW-S wash solution that is contained in the kit. For further information, read instruction contained in the kit.
- 2) Weigh and label final catch tubes (contained in the kit, look like 2 ml eppis).
- 3) After taking out your soil samples (~400 mg) from the -80°C freezer put them immediately on ice and transfer them to the lab. Prevent them from thawing.
- 4) Transfer frozen soil samples into pre-weighed Lysing matrix E tubes and weigh them if you lose a lot of soil during transferring it (in order to know the exact amount of soil that you extracted the DNA from).
- 5) Add 978 µl Sodium Phosphate Buffer (contained in the kit) to sample in Lysing Matrix E tube.
- 6) Add 122 µl MT buffer (contained in the kit).
- 7) Homogenize by using the bead beater.
Settings: time= 30 seconds; speed= 4.5
- 8) Centrifuge at max speed (=12500 rpm) for 15 min to pellet debris. Centrifuge should be cooled! (Because it takes some time, until the centrifuge has cooled down, turn it on in the morning!)
- 9) Transfer supernatant (in the steps: 2 x 400 µl) to a clean 2 ml Eppi. If it is, for some reason not possible to add 2x 400 µl, then add as much as possible but note exact amount of supernatant that you have transferred. This information is critical for the calculation-steps afterwards.
- 10) Add 250 µl PPS (Protein Precipitation Solution, contained in the kit) and mix by shaking the tubes gently by hand (10 complete inversions and 20 x gently shaking up and down.)
- 11) Centrifuge at max speed (=12500 rpm) for 5 minutes to let the pellet precipitate.
Transfer supernatant (in steps: 2 x 500 µl) to a clean 15 ml tube Greiner tube or to a 5ml Eppi. If it is, for some reason not possible to add 2x 500 µl, then add as much as possible but note exact amount of supernatant that you have transferred. This information is critical for the calculation-steps afterwards.
- 12) Resuspend Binding Matrix suspension (contained in the kit) by rigorously shaking and add 1 ml of it to the supernatant in the 15 ml Greiner/the 5 ml Eppi.
- 13) Invert samples gently by hand for 3 minutes to allow binding of DNA.
- 14) Resuspend Binding Matrix contained the supernatant by shaking 3 times vertically and 3 times horizontally before doing the following step:
 - a) Transfer 800 µl of the resuspended mixture from the 15 ml Greiner vial/5 ml Eppi to a spin TM filter tube (contained in the kit) and centrifuge at max speed (=12500 rpm) for 5 minutes. Centrifuge should be cooled. Empty the catch tube, put the filter back into the sample catch tube but move it 180°, so that the pellet is not only forced in one direction during the centrifugation step. However, this step is not obligatory, just helpful.
 - b) Transfer 700 µl of the resuspended mixture from the 15 ml Greiner vial/5 ml Eppi to spin TM filter tube and centrifuge at max speed (=12500 rpm) for 5 minutes. Centrifuge should be cooled. Empty the catch tube, put the filter back into the sample catch tube but move it 180°, so that the pellet is not only forced in one direction during the centrifugation step. However, this step is not obligatory, just helpful.
 - c) Transfer 400 µl of the resuspended mixture from the 15 ml Greiner vial/5 ml Eppi to spin

TM filter tube and centrifuge at max speed (=12500 rpm) for 5 minutes. Centrifuge should be cooled. Empty the catch tube, put the filter back into the same catch tube but move it 180°, so that the pellet is not only forced in one direction during the centrifugation step. However, this step is not obligatory, just helpful.

- 15) Add 500 µl of the prepared SEWS-M solution (see step 1) and gently resuspend the precipitate on the filter by only using the force of the liquid from the pipette tip.
Make sure not to shake the vial, just push liquid up and down a few times with the pipette, so that the added clear solution on the filter gets white-ish. Take care not to scratch the filter with the pipette tip!
- 16) Centrifuge at max speed (=12500 rpm) for 2 minutes. Centrifuge should be cooled.
- 17) Empty the catch tube and put the filter into the same catch tube again.
- 18) Without any addition of liquid, centrifuge again at max speed (=12500 rpm) for 5 minutes to dry the matrix of residual wash solution. Centrifuge should be cooled. Discard the catch tube and put the filter into the new, pre-weighed clean catch tube.
- 19) Air dry the spin filter for 5 minutes at room temperature in the catch tube (just open the catch tube).
- 20) Gently resuspend Binding Matrix on the spin filter in 100 µl of DNase Pyrogen-free Water (DES; contained in the kit). Again, this is done only by using the force of the liquid from the pipet tip. Make sure not to shake the vial, just push liquid up and down a few times with the pipette, so that the added clear solution on the filter gets white-ish. Take care not to scratch the filter with the pipette tip!
- 21) Centrifuge at max speed (=14000 rpm) for 2 minutes to bring eluted DNA into the clean catch tube. Centrifuge should be cooled.
- 22) Discard the spin filter and keep the solution (= DNA extract) at the bottom.
the DNA extract is now ready for downstream applications.
- 23) Weigh DNA extract yield in catch tube and note (yield should be around ~80 µl).
- 24) (Pipette 10 µl of the DNA extract into a small DNase-free screw cap vial for further Pico-green analysis.
- 25) Pipette the remaining DNA extract into a small DNase-free screw cap vial for further ¹⁸O-analysis.
(This step avoids that the DNA extracts gets thawed several times, which is always critical for analysis of ¹⁸O contents.)
- 26) Store at -80°C for extended periods.

C DNA quantification and quality check: Gels

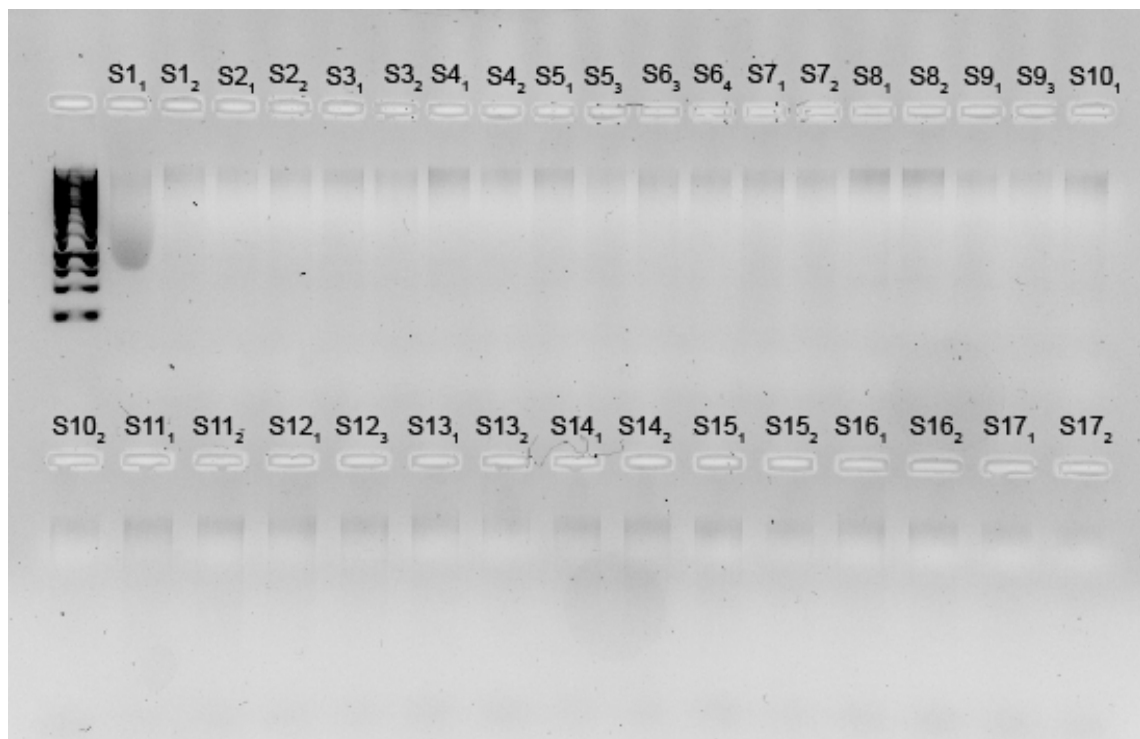


Figure 22 Quality check of the DNA of the extraction replicates of the start samples. Replicate 1 of S1 had a smear and was subsequently not used for the 16S amplicon sequencing. All other replicates showed DNA bands.

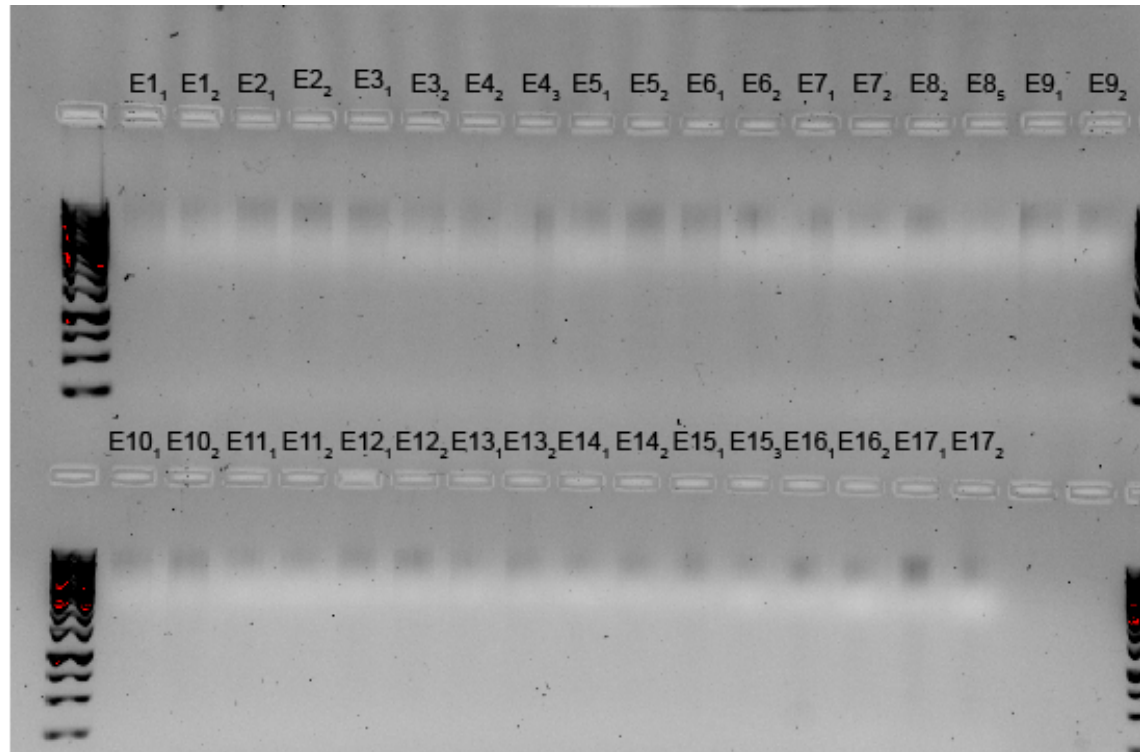


Figure 23 Quality check of the DNA of the extraction replicates of the end samples. All replicates showed DNA bands.

D 16S Amplicon sequencing: Percentage coverage of primers

The percentage coverage of the A519F and the Bakt_805R primers used in this study for the 16S amplification prior to sequencing.

IMGM Laboratories GmbH
Bunsenstr. 7a
D-82152 Martinsried
Germany

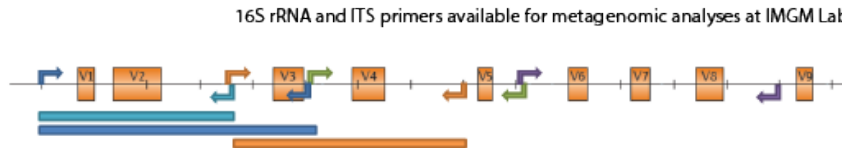


Fig. 1: Graphical overview of primers and their position along the 16S rRNA sequence. Five possible combinations suitable for MiSeq sequencing are depicted using different colours.

Region	Primer	direction	Sequence 5'-3'	coverage (no mismatch) ^a			coverage (one mismatch) ^a		
				Archaea (A)	Bacteria (B)	Eukaryota (E)	Archaea (A)	Bacteria (B)	Eukaryota (E)
16S Bacteria specific									
V1-2	8F-YM	forward	AGAGTTTGATYMTGGCTCAG	0.0	83.6	0.0	0.0	92.2	0.0
	Bakt_357R	reverse	CTGCWCCNCCCGTAGG	0.5	94.9	0.0	66.6	98.1	0.2
V1-3	8F-YM	forward	AGAGTTTGATYMTGGCTCAG	0.0	83.6	0.0	0.0	92.2	0.0
	517R	reverse	ATTACCGCGCTGCTGG	0.5	87.6	86.2	30.9	97.8	93.3
V3-4	Bakt_341F	forward	CCTACGGNGGCWGAG	0.5	94.9	0.0	66.6	98.1	0.2
	Bakt_805R	reverse	GACTACHVGGGTATCTAAC	90.1	90.4	0.0	96.5	98.2	0.8
V4-5	U515F	forward	GTGCCAGCMGCCGCGTAA	54.5	95.4	92.2	96.2	98.4	97.0
	908R	reverse	CGTCAAATTCTTGTAGTT	0.0	89.9	0.0	0.9	97.0	77.6
V6-8	909F	forward	ACTCAAAGAAATWGACGG	0.0	91.7	0.1	0.9	97.5	77.8
	1391R	reverse	GACGGCCGGTGWGTRCA	72.7	84.6	93.5	76.0	87.8	96.1
16S Archaea specific									
V3-4	Arch349F	forward	GYGCASCAGKCGMGAAW	79.6	0.0	0.0	92.4	0.0	0.1
	A806R	reverse	GGACTACVSGGGTATCTAAT	87.4	7.8	0.0	96.5	92.1	0.1
V4-5	A519F	forward	CAGCMGCCGCGTAA	95.2	95.7	92.7	97.7	98.4	97.2
	U906R	reverse	CAATTCTTAAAGTTTC	83.7	0.3	76.9	93.2	49.8	96.3
V4	A519F	forward	CAGCMGCCGCGTAA	95.2	95.7	92.7	97.7	98.4	97.2
	Bakt_805R	reverse	GACTACHVGGGTATCTAAC	90.1	90.4	0.0	96.5	96.2	0.8

Tab. 1: List of 16S primers for bacterial or archaeal specific amplification. The amplified regions are also presented in Fig. 1 using the corresponding colour. Primer sequences and the coverage (%) are described as in reference Klindworth et. al 2013. High primer coverage is coloured in green, moderate coverage in yellow and low coverage in red.

Appendix II: Results

A Linear regression plot of CH₄ concentrations

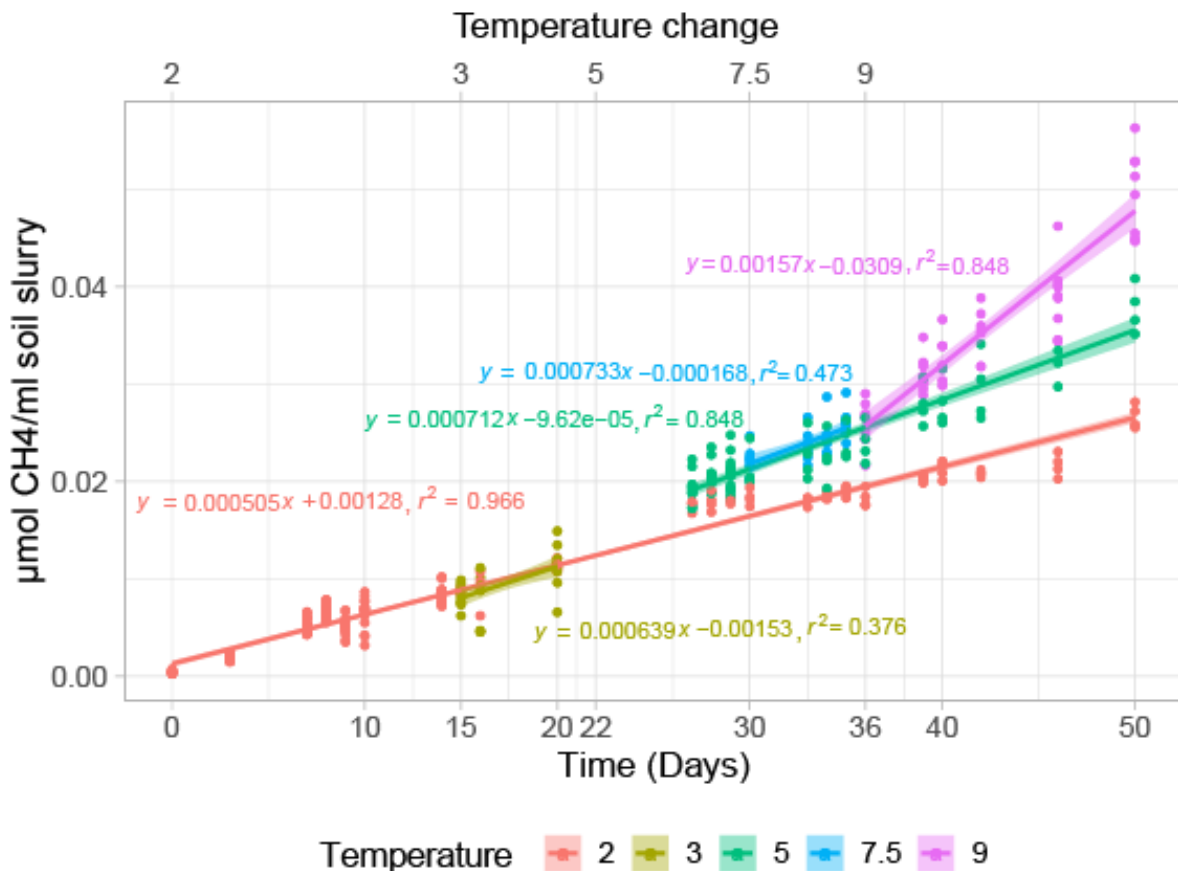


Figure 24 Linear regression models fitted for each temperature treatment. Red is for the 2°C incubations, yellow is for the 3°C incubations, green is the 5°C incubations, blue is the 7.5°C incubations and purple is for the 9°C incubations.

B Biphasic CH₄ production rates

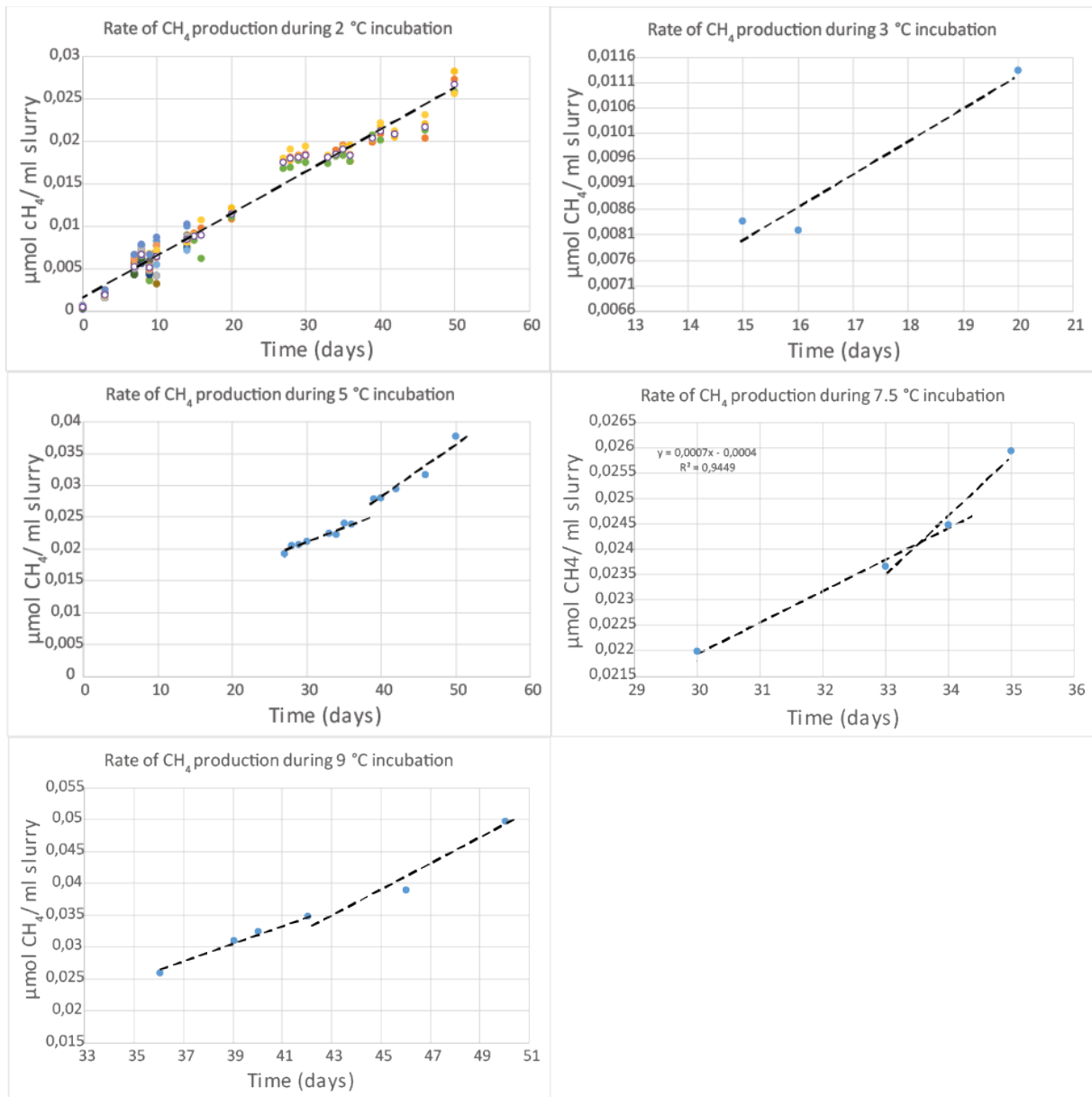


Figure 25 The average concentration of CH₄ for each temperature treatments plotted against time. Black, stippled lines shows how the biphasic rates were calculated. These are not exact, just indications of how it was done. All samples of the 2°C were plotted along with the average to confirm that the average was a good representation of all the samples. The rates for the 2°C and 3°C were not treated as biphasic.